Defective bicarbonate reabsorption in Kir4.2 potassium channel deficient mice impairs acid-base balance and ammonia excretion

Yohan Bignon, Laurent Pinelli, Nadia Frachon, Olivier Lahuna, Lucile Figueres, Pascal Houillier, Stéphane Lourdel, Jacques Teulon, Marc Paulais

Defective bicarbonate reabsorption in Kir4.2 K^+ channel-deficient mice impairs acid-base balance and ammonia excretion

Methods

Renal ammonia metabolism was studied in a model of mice deleted for Kir4.2.

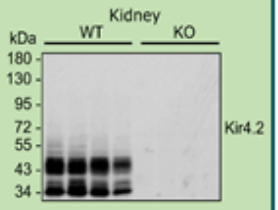

Results

Kir4.2 deletion depolarized the proximal cell membrane, increased pH_i, impaired ammoniagenic enzymes and ammonia excretion, and caused isolated pRTA.

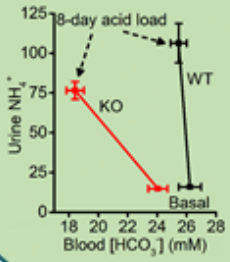

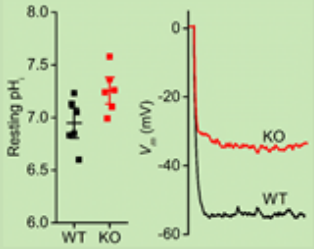

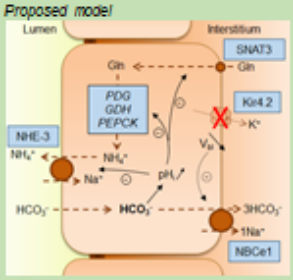

CONCLUSION: Kir4.2(*Kcnj15*) regulates ammonia metabolism in mouse proximal tubule. *KCNJ15* may be a new candidate gene for human isolated pRTA.

ISN kidney INTERNATIONAL
OFFICIAL JOURNAL OF THE INTERNATIONAL SOCIETY OF NEPHROLOGY

Bignon et al, 2019

Defective bicarbonate reabsorption in Kir4.2 potassium channel deficient mice impairs acid-base balance and ammonia excretion

Yohan Bignon[1,2], Laurent Pinelli[1,2], Nadia Frachon[1,2], Olivier Lahuna[3], Lucile Figueres[1,2], Pascal Houillier[1,2], Stéphane Lourdel[1,2], Jacques Teulon[1,2] and Marc Paulais[1,2]

[1]Centre de Recherche des Cordeliers, INSERM, Sorbonne Université, Université Sorbonne Paris Cité (USPC), Université Paris Descartes, Université Paris Diderot, Paris, France

[1]Centre National de la Recherche Scientifique (CNRS), ERL 8228, Paris, France.

[3]INSERM U-1016, Institut Cochin, Paris, France.

Corresponding author: Marc Paulais, ERL 8228, Centre de Recherche des Cordeliers, 15 rue de l'école de médecine, 75270 PARIS CEDEX 06, France.

E-mail: marc.paulais@inserm.fr

Running title: Kir4.2 and renal ammoniagenesis

ABSTRACT

The kidneys excrete the daily acid load mainly by generating and excreting ammonia but the underlying molecular mechanisms are not fully understood. Here we evaluated the role of the inwardly rectifying potassium channel subunit Kir4.2 (*Kcnj15* gene product) in this process. In mice, Kir4.2 was present exclusively at the basolateral membrane of proximal tubular cells and disruption of *Kcnj15* caused a hyperchloremic metabolic acidosis associated with a reduced threshold for bicarbonate in the absence of a generalized proximal tubule dysfunction. Urinary ammonium excretion rates in *Kcnj15*- deleted mice were inappropriate to acidosis under basal and acid-loading conditions, and not related to a failure to acidify urine or a reduced expression of ammonia transporters in the collecting duct. In contrast, the expression of key proteins involved in ammonia metabolism and secretion by proximal cells, namely the glutamine transporter SNAT3, the phosphate-dependent glutaminase and phosphoenolpyruvate carboxykinase enzymes, and the sodium-proton exchanger NHE-3 was inappropriate in *Kcnj15*-deleted mice. Additionally, *Kcnj15* deletion depolarized the proximal cell membrane by decreasing the barium-sensitive component of the potassium conductance and caused an intracellular alkalinization. Thus, the Kir4.2 potassium channel subunit is a newly recognized regulator of proximal ammonia metabolism. The kidney consequences of its loss of function in mice support the proposal for *KCNJ15* as a molecular basis for human isolated proximal renal tubular acidosis.

Key words: Ammoniagenesis; Isolated metabolic acidosis; Kir4.2 potassium channel; Proximal tubule

TRANSLATIONAL STATEMENT

Chronic metabolic acidosis caused by a failure to adapt renal ammonia excretion to the daily net acid load is an independent risk factor for the progession of the chronic kidney disease towards end-stage renal disease and is significantly associated with higher mortality. We report a new molecular actor in ammonia metabolism whose defect leads to isolated proximal renal tubular acidosis in mice. This study may shed more light on the pathophysiology of this inherited disease and improve our understanding of the mechanisms underlying acid-base regulation in human health and disease; it also may also provide a basis for accurate clinical and genetic diagnosis and future design of targeted therapeutics along with, possibly, strategies for gene therapy of this disorder.

INTRODUCTION

Commonly associated is with chronic kidney disease, metabolic acidosis accelerates the progression of chronic kidney disease to end-stage renal disease and leads to higher mortality.[1] Renal ammonia[a] metabolism is a cornerstone of kidney's ability to excrete acid, and a declining ability to excrete the daily net acid load because a failure to adapt renal ammonia excretion is an independent risk factor for the progession of chronic kidney disease toward end-stage renal disease.[2] (In this article, the term "ammonia" refers to the combination of NH_3 and NH_4^+. The term "NH_3" or "NH_4^+" is used only when referring to a specific molecular form.) Because most of the excreted ammonia arises from its production and secretion by proximal tubular cells, deciphering the events governing proximal ammonia metabolism is of fundamental importance for comprehending the pathophysiology of disorders involving renal acid excretion.

Information regarding regulation of ammonia metabolism during proximal renal tubular acidosis (pRTA) is limited and mainly arose from clinical studies of patients with permanent forms of familial isolated pRTA. This rare acid-base disturbance, although primarily defined by a failure to reabsorb filtered HCO_3^- in the absence of a generalized proximal tubule dysfunction, is also associated with inappropriately low urinary NH_4^+ excretion rates under basal and acid-loading conditions.[3] To date, only the Na^+-HCO_3^- cotransporter NBCe1, whose loss of function by mutations in solute carrier family 4 member 4 *SLC4A4* causes the most common form of isolated pRTA, has been identified as a critical actor in abnormal ammonia metabolism in this disease. Thus *Slc4a4* deletion in mice causes severe pRTA and impairs urinary NH_4^+ excretion by reducing the proximal expression of ammoniagenic enzymes.[4,5,6] However, the finding that rarer cases of isolated pRTA occur independently of *SLC4A4* mutations indicates that other regulators of renal ammonia metabolism may be involved in the reduced NH_4^+ excretion in this disease.[7]

Early studies in mice suggested that the basolateral potassium conductance of proximal tubular cells might be a key player in the regulation of ammonia metabolism.[8,9] Several potassium channel subunits that may underlie this conductance have been dentified on a molecular level, including the inwardly rectifying Kir4.2 (*Kcnj15)* subunit.[10] Here, we used a new strain of mice in which *Kcnj15* is deleted and demonstrate that basolateral Kir4.2 is a major determinant of the membrane potential of proximal cells and regulates ammonia metabolism. These results provide further insight into the molecular mechanisms involved in renal acid-base homeostasis and support *KCNJ15* as a new candidate for yet unelucidated isolated proximal metabolic acidoses.

RESULTS

Validation of mice with deletion of *Kcnj15*. Adult mice carrying a disrupted *Kcnj15* gene were obtained as detailed in the Supplementary Methods section. The successful incorporation of the mutant allele was established by polymerase chain reaction (PCR) on genomic DNA from tail biopsies (Figure 1a), and the absence of native Kir4.2 protein in *Kcnj15*$^{-/-}$ mice was confirmed by Western blot analysis of kidneys (Figure 1b), as well as in lung and stomach where Kir4.2 is also present.[11] In the kidney of *Kcnj15*$^{+/+}$ mice, major Kir4.2-specific bands were observed near the predicted molecular mass of the monomeric peptide[12] and corresponding to its glycosylation status as observed by others on mouse renal cortex using the same Kir4.2 antibody.[13]

Cellular distribution and subcellular localization of renal Kir4.2. In accordance with observations in the human kidney,[14] real-time PCR on glomeruli and tubular segments isolated from kidneys of *Kcnj15*$^{+/+}$ mice revealed Kir4.2 mRNA expression exclusively in the convoluted and straight portions of the proximal tubule (Figure 2a). The Kir4.2 peptide was detected in renal cortical and subcortical regions (Figure 2b) and more specifically in proximal cells of cortex and outer stripe of the outer medulla (Figure 2c). No Kir4.2 labeling was observed in the inner stripe of the outer medulla devoid of proximal tubule (Figure 2d). In cortical cells of *Kcnj15*$^{+/+}$ mice, the Kir4.2 peptide was observed in a region ranging from the basal side up to nearly two thirds of cell height, likely corresponding to basolateral membrane infoldings, leaving unstained a shallow subapical region and microvilli (Figure 3a). The Kir4.2 immunofluorescence intensity profile peaked at 1.6 ± 0.3 µm (n = 13 cells) away from the basal pole (Figure 3b), indicating a basolateral localization.

Phenotype of mice with *Kcnj15* deletion. *Kcnj15*$^{-/-}$ mice exhibited no excess mortality or detectable growth retardation and were indeed indistinguishable from their *Kcnj15*$^{+/+}$ littermates

by gross physical appearance (Supplementary Figure S1). Their daily water and food intakes were normal (P = 0.67 and 0.71, respectively, vs *Kcnj15*$^{+/+}$ mice) and their kidneys showed no alteration in gross external appearance and weight and no morphologic or ultrastructural abnormality (Suplementary Figure S1).

Analyses of plasma and urine of *Kcnj15*$^{-/-}$ mice revealed no sign of polyuria, salt wasting, or elevated fractional excretions of phosphate, glucose and proteins; in addition, their normal estimated glomerular filtration rate indicated no chronic renal failure (Tables 1 and 2). In contrast, *Kcnj15*$^{-/-}$ mice were spontaneously acidotic. Their lower blood HCO_3^- concentration was counterbalanced by an equivalent increase in plasma Cl^- concentration (Figure 4a), which, together with normal plasma Na^+ and K^+ concentrations (Table 1), yielded a normal plasma anion gap. *Kcnj15*$^{-/-}$ mice also spontaneously produced an acidic urine (P < 0.0001 vs *Kcnj15*$^{+/+}$ mice) with a barely significant HCO_3^- wasting (P < 0.04 vs *Kcnj15*$^{+/+}$ mice; Figure 4b). To determine whether this minimal HCO_3^- loss reflected a new steady state where blood HCO_3^- content was lowered to a value close to a reduced renal threshold for HCO_3^-, mice were challenged with 24-hour HCO_3^- loads. In these conditions, the HCO_3^- filtered loads in the two groups of mice were similar (Supplementary Table S1) and urinary pH increased because bicarbonaturia occurred when blood HCO_3^- concentration rose above their respective renal threshold for HCO_3^- (Figure 4b). Nevertheless, urine alkalinization and bicarbonaturia in *Kcnj15*$^{-/-}$ mice appeared at blood HCO_3^- concentrations that were lower than the low normal range in *Kcnj15*$^{+/+}$ mice, highlighting a reduced renal threshold for HCO_3^-. In the absence of a generalized proximal dysfunction (described previously), *Kcnj15* deletion therefore caused an isolated pRTA.

NH_4^+ excretion under basal and exogenous acid-loading conditions. Under basal conditions, *Kcnj15*$^{-/-}$ mice did not exhibit the expected increase in urinary NH_4^+ content in response to acidosis and only slightly increased net acid excretion (Figure 5a), as expected from

an acidosis of tubular origin. To determine whether they were able to excrete maximal amounts of NH_4^+, *Kcnj15*$^{-/-}$ mice were challenged with a 8-day exogenous NH_4Cl load. After 2 days, *Kcnj15*$^{-/-}$ mice exhibited almost 2-fold greater changes in blood pH and blood HCO_3^- and plasma Cl^- concentrations than did *Kcnj15*$^{+/+}$ mice ($P < 0.05$ for each parameter; Figure 5b), despite a ~ 20 % lower acid load (Supplementary Figure S2), likely due to a reduced water intake (Supplementary Table S2). Then, wheras *Kcnj15*$^{+/+}$ mice completely recovered at day 8 of the acid-loading period, *Kcnj15*$^{-/-}$ mice remained acidotic ($P < 0.05$ vs day 0 for blood pH and for blood HCO_3^- and plasma Cl^- concentrations; n = 5-10). All along the treatment period, the urinary NH_4^+ excretion rate in *Kcnj15*$^{-/-}$ mice progressively increased but remained one-third lower than in *Kcnj15*$^{+/+}$ mice ($P < 0.001$, analysis of variance; Figure 5c). Actually, *Kcnj15* deletion reduced by a factor of ~ 10 the sensitivity of the changes in urinary NH_4^+ excretion to the degree of metabolic acidosis (in mmol urinary NH_4^+/mmol creatinin per mM blood HCO_3^- : 117 in *Kcnj15*$^{+/+}$ mice vs 11 in *Kcnj15*$^{-/-}$ mice). Also, the urinary pH in *Kcnj15*$^{-/-}$ mice remained more acidic than in *Kcnj15*$^{+/+}$ mice all throughout the acid-loading period (Figure 5d), indicating an intact ability to achieve a high urine free H^+ concentration but not matched by an appropriate NH_4^+ excretion.

The mRNA levels for the rhesus proteins RhBG and RhCG, 2 major transporters involved in final urinary ammonia secretion by distal cells,[15] were normal in *Kcnj15*$^{-/-}$ mice (Supplementary Figure S3). Also, *Kcnj15*$^{-/-}$ mice fully concentrated their urine under basal and acid-loading conditions (Table 2 and Supplementary Table S2), indicating an intact medulla, a prerequisite for the accumulation of NH_3 into the interstitium, facilitating its transfer into the collecting duct lumen.[16] These results excluded a low NH_4^+ excretion related to a defective distal nephron in *Kcnj15*$^{-/-}$ mice and altogether pointed toward a defect in proximal ammoniagenesis.

Expression of enzymes and transporters relevant for ammoniagenesis. Ammoniagenesis in the proximal tubule arises from the basolateral uptake of glutamine and its metabolism by a series of mitochondrial and cytosolic enzymes, both highly upregulated by metabolic acidosis or an exogenous acid load.[17,18] We first performed quantitative reverse transcription PCR on whole kidney preparations for the basolateral transporter system N1 Na^+ and H^+-coupled glutamine transporter (SNAT3), the phosphate-dependent glutaminase (PDG), glutamate dehydrogenase (GDH), and phosphoenolpyruvate carboxykinase (PEPCK) enzymes, and the apical Na^+/H^+ exchanger (NHE-3), the primary pathway for NH_4^+ secretion by proximal tubular cells. Compared with *Kcnj15*$^{+/+}$ mice, the basal mRNA abundance of SNAT3 and PEPCK was reduced in *Kcnj15*$^{-/-}$ mice, with those of PDG, GDH remaining unchanged (Figure 6). In addition, the response of *Kcnj15*$^{-/-}$ mice to the acid load was significantly blunted for SNAT3, GDH and PEPCK and absent for PDG. In contrast, the mRNA for the broad neutral (0) amino acid transporter 1 (B^0AT1) and L-type amino acid transporter 2 (LAT2) transporters, typically involved in glutamine reabsorption, were only marginally affected by *Kcnj15* deletion and the acid load (Supplementary Figure S4). Lastly, NHE-3 mRNA abundance in *Kcnj15*$^{-/-}$ mice under basal and acid-loading conditions was similar to that in *Kcnj15*$^{+/+}$ mice.

We substantiated these observations by Western blots experiments; the results are summarized in Figure 7. Under basal condition, PEPCK, PDG and NHE-3 proteins abundance in *Kcnj15*$^{-/-}$ mice was in accordance with results on mRNA levels, whereas that of SNAT3 was more elevated than in *Kcnj15*$^{+/+}$ mice, opposite to our mRNA data. In addition, PEPCK peptide expression in acid-loaded *Kcnj15*$^{-/-}$ mice followed enzyme mRNA level, whereas that of SNAT3, PDG and NHE-3 did not exhibit the higher protein levels expected from the more severe acidosis in this condition.

Intracellular pH, membrane potential and NBCe1 expression determination. It has been early suggested that the reduced rate of ammonia excretion in patients with isolated pRTA might originate from an increase in intracellular pH (pH_i), possibly caused by an impaired basolateral exit of HCO_3^-.[19] As summarized in Figure 8a, the resting pH_i of cells bathed in a Na^+- and HCO_3^--containing solution was significantly higher, that is more alkaline, in *Kcnj15*$^{-/-}$ mice (7.26 ± 0.1, n = 6 tubules from 4 mice) than in *Kcnj15*$^{+/+}$ mice (6.95 ± 0.1, n = 6 tubules from 4 mice) (P = 0.036). The blockade of the basolateral Na^+-HCO_3^- exit from proximal cells increasing pH_i,[20] a decreased expression of NBCe1, responsible for the basolateral exit of HCO_3^- out of proximal tubular cells,[3] or of the TWIK-related acid-sensitive K^+ channel 2 (Task2) potassium channel, proposed to sustain the activity of the rheogenic NBCe1,[21] could have accounted for the alkaline pH_i in *Kcnj15*$^{-/-}$ mice. However, *Kcnj15* deletion leaved unchanged NBCe1 and Task2 mRNA levels (Supplementary Figure S5) and did not decrease their respective protein abundance, with that of NBCe1 even increasing (Figure 8b).

Because a depolarization of the basolateral membrane of proximal tubular cells, induced by high bath K^+ concentration or the addition of barium, causes an intracellular alkalinization dependent on basolateral Na^+-HCO_3^- transport,[22,23] the impact of *Kcnj15* deletion on membrane potential (V_m) was then investigated (Figure 8c). In *Kcnj15*$^{+/+}$ mice, the resting V_m was -52 ± 2.5 mV (n = 14 patches from 6 mice), in reasonnable agreement with values measured in mice using microelectrodes,[24,25] and markedly less negative with 1 mM barium in the bath (V_m = -21 ± 2.4 mV, n = 6 patches from 4 mice). At rest, the proximal cell membrane of *Kcnj15*$^{-/-}$ mice was significantly depolarized (V_m -32 ± 3.1 mV ; n = 16 patches from 10 mice) and bath barium had a reduced effect (V_m = -21 ± 1.9 mV, n = 6 patches from 4 mice). We next attempted to evaluate the impact of *Kcnj15* deletion on the rheogenic NBCe1 activity by using conditions producing changes in pH_i whose magnitude and rate constant reflect the basolateral Na^+-HCO_3^-

cotransport.[26,27] Original pH_i recordings are shown in Figure 8d, and the detailed kinetics analysis of the changes in pH_i is given in Table 3. Stimulating either Na/HCO_3 exit by bath Na^+ withdrawal or then entry by bath Na^+ readdition in *Kcnj15*$^{+/+}$ and *Kcnj15*$^{-/-}$ mice caused respective initial changes in pH_i with statistically similar kinetics, although quite variable from tubule to tubule within a group of mice. Nevertheless, while pH_i either remained stable under Na^+-free condition (3 tubules, see Figure 8d) or slightly recovered (3 tubules; not shown) in *Kcnj15*$^{+/+}$ mice, it rose at or above its initial resting level (2 tubules, see Figure 8d) or partially recovered (3 tubules; not shown). Therefore, the presence of a pH_i regulatory mechanism in *Kcnj15*$^{-/-}$ mice, despite the absence of luminal and bath Na^+, together with the more alkaline pH_i values, precluded further computational analysis of our data in terms of Na/HCO_3 transport rates and NBCe1 activity. (The amplitude and rate constant of the pH_i changes cannot be taken from experiments in which pH_i regulatory mechanisms are still operating and may lead to underestimates. In addition, the amplitude of the changes in pH_i is also inversely proportional to the intracellular buffering power [β] which depends on pH_i.)

DISCUSSION

The basolateral membrane conductance of mouse proximal cells is almost purely selective to K^+ and markedly inhibited by barium.[24,28] Our results show that the inwardly rectifying Kir4.2 subunit underlies almost two thirds of the whole membrane barium-sensitive potassium conductance. In our experimental conditions, luminal potassium channels may have contaminated our membrane potential measurements in the presence of barium,[10] but given that the basolateral membrane potassium conductance is much higher than that of the luminal membrane,[24] such a contamination would be minimal and, in any case, have led to an underestimation of the contribution of Kir4.2 to the basolateral membrane potassium conductance.

A barium-sensitive conductive transport of NH_4^+ across the basolateral membrane of mouse proximal cells may contribute to its cellular uptake.[9] Although the permeability of Kir4.2 to NH_4^+ has not been established, it is legitimate to consider that, as for most potassium channels, NH_4^+ can permeate Kir4.2 and that *Kcnj15* deletion could have contributed to the impaired NH_4^+ secretion. Nevertheless, such a conductive influx of NH_4^+ into proximal cells is predicted to remain very limited, even assuming a relatively high P_{NH4}/P_K of ~ 0.3 (the P_{NH4}/P_K of the Kir4.1 channel is only ~ 0.1).[29,30] Lastly, the decreased basolateral potassium conductance in the absence of Kir4.2 could have altered Na^+/K^+-adenosine triphosphatase activity and NH_4^+ entry, through its substitution for K^+ at the K^+ binding site,[31,32] but kinetic models suggest a potentially significant NH_4^+ transport by this pathway only in the inner medulla,[30,31] devoid of proximal tubule.

The reduced sensitivity of the changes in urinary NH_4^+ excretion to the degree of metabolic acidosis in mice with deletion of *Kcnj15* was more clearly associated with the inappropriate expression of major ammoniagenic enzymes under basal and acid-loading conditions. Of note, the marked decrease in PEPCK expression would raise intramitochondrial

glutamate and α-ketoglutarate contents and further decrease PDG and GDH activities by competitive inhibition.[33] In addition, the inappropriate protein expression of SNAT3 under acid-loading condition likely blunted glutamine uptake and availability for ammoniagenesis. Whereas the increased basal expression of SNAT3 would favor glutamine uptake and ammoniagenesis, as expected from spontaneously acidotic mice,[17] SNAT3 transports glutamine with Na^+ in exchange for H^+ so that the rise in pH_i we observed in mice with deletion of *Kcnj15* would decrease the chemical gradient for H^+ and blunt glutamine uptake.[34] That *Kcnj15* deletion also may impair NH_4^+ secretion by NHE-3 remains unclear. Because acidosis increases NHE-3 protein expression in cells of proximal tubules and thick ascending limb,[35,36] all or part of the inappropriate NHE-3 expression in mice with deletion of *Kcnj15* cannot yet be precisely assigned to either nephron segment. In any case, since NHE-3 in thick ascending limbs cells is supposed to secrete NH_4^+,[16] its reduced expression in the proximal tubule and/or in the TAL would ultimately lower the NH_4^+ content of the final urine.

In patients with isolated pRTA, the low NH_4^+ excretion rates are thought to result from an intracellular alkalinization.[19] The increased pH_i in proximal cells of mice lacking Kir4.2 supports this hypothesis. In patients carrying loss-of-function mutations in *SLC4A4*, as well as in mice where *Slc4a4* deletion impairs urinary NH_4^+ excretion by the reduced expression of ammoniagenic enzymes,[4,5,20] the most straightforward explanation to an elevated pH_i would be an intracellular accumulation of HCO_3^- caused by the absence of NBCe1 at the cell membrane. Our observation that *Kcnj15* deletion did not decrease NBCe1 protein expression suggests another mechanism. (Acidosis notoriously has no effect on the expression of the major NBCe1-A isoform protein in the cortex but increases the expression of the minor NBCe1-B isoform in the outer stripe of the outer medulla. The increased NBCe1 protein expression we observed thus may

reflect the upregulation of NBCe1-B.) Notably, NBCe1 is rheogenic rendering both the magnitude and polarity of basolateral HCO_3^- transport sensitive to changes in membrane potential.[37] In particular, a depolarization decreases NBCe1-dependent HCO_3^- exit from proximal cells and increases pH_i.[22,37,38] The depolarized proximal cell membrane of mice with deletion of *Kcnj15*, lower threshold for HCO_3^-, and increased pH_i are all consistent with a reduced NBCe1 activity by a voltage-dependent effect. Nevertheless, the involvement of an additional, possibly depolarization-activated, pH_i regulatory mechanism cannot be excluded and additional studies will be required to differentiate between these mechanisms.

To date, only the Task2 channel was proposed to sustain NBCe1 activity in proximal tubular cells.[21] Although urinary ammonia excretion was not evaluated in *Kcnk5*(Task2)-deleted mice, the present study indicates that proximal HCO_3^- reabsorption and ammoniagenesis may be regulated by multiple potassium channels types. At present, the respective contributions and concerted actions of Kir4.2 and Task2 remain to be determined because the loss of function of each of them leads to isolated pRTAs of similar severity. This notwithstanding, the phenotype of mice with deletion of *Kcnj15*, mild compared with that in mice with homozygous NBCe1 deletion,[4] was not attenuated by the over-expression of Task2. Actually, the acidosis in mice lacking Kir4.2 is comparable to the severity of the acid-base disturbance caused by haploinsufficiency in *Slc4a4*,[4,6] and appears consistent with reports showing that a decreased transport by NBCe1 is sufficient to cause pRTA.[39]

In summary (Figure 9), Kir4.2 is a major component of the basolateral barium-sensitive potassium conductance in proximal cells and a new molecular entity through which the kidneys regulate proximal ammonia metabolism, with its loss of function causing a membrane depolarization, an increase in pH_i, and a reduced ammoniagenesis. The rise in pH_i and lowered

threshold for HCO_3^- in mice with deletion of *Kcnj15* strongly indicate a reduced driving force for the NBCe1-mediated Na^+-HCO_3^- transport as a result of membrane depolarization.

The renal phenotype of mice invalidated for *Kcnj15* recapitulates the clinical features of patients with isolated pRTA.[40,41,42] Thus mice with deletion of *Kcnj15* spontaneously develop a pRTA in the absence of a generalized proximal dysfunction, that is, outside a Fanconi syndrome, and do not exhibit the expected increases urinary NH_4^+ excretion under basal and acid-loading conditions. This makes our observations relevant to human renal physiology and improves our comprehending of acid-base homeostasis and ammonia metabolism. By supporting *KCNJ15* as a candidate for human pRTA, our results also bring new insight to the yet unidentified genetic cause of disorders in patients with mild isolated pRTA and lacking mutation in *SLC4A4*.[7,40]

In cells of the distal convoluted tubule, the closely related Kir4.1 subunit is currently viewed as part of a basolateral K^+ sensor translating K^+ homeostasis to regulation of NaCl reabsorption.[43] This study expands our view on the functionally relevant renal Kir channels to the proximal tubule and the emergence of Kir4.2 as K^+-to-voltage sensor, possibly intimately linking acid-base balance and ammonia metabolism to K^+ intake,[44] may be anticipated.

METHODS

Mice. Animals were handled in full compliance with the french government welfare policy. The scientific project and the experimental procedures were favorably evaluated by the Charles Darwin Ethics Committee for animal experimentation (Permit 03-MP/8569/[0]). Mice were housed in the Centre d'Explorations Fonctionnelles (UMRS1138, Paris, France; Permit B75-06-12) and the confined usage of genetically modified organisms (Class 1) was registered with the french Ministère de l'Education Nationale, de l'Enseignement Supérieur et de la Recherche.

Adult mice were fed with pellets of a complete 0.25% Na^+, 0.6% K^+, 0.73% Ca^{2+} SAFE-A04 maintenance diet (Usine d'Alimentation Rationnelle, Augy, France) with free access to tap water until the beginning of the experiment. Kidneys retrievals were performed on mice anesthetized by the intraperitoneal injection of ketamine (0.12 mg/g body weight) and xylazine (6 µg/g body weight).

Metabolic studies. Metabolic studies were performed in individual metabolic cages (Tecniplast, Decines Charpieu, France) on adult male mice fed with SAFE-A04 powder chow with free access to deionized water alone or supplemented with either 0.28M NH_4Cl, 0.1 M or 0.28 M $NaHCO_3^-$ and 0.3M sucrose, when appropriate. The methods used for collections and analyses of urine and blood samples were as previously described,[45] with the modifications detailed in Supplementary Methods section.

Real-time PCR. Real-time PCR on microdissected glomeruli and tubular segments and quantification were as previously described.[46,47] The procedure used for the extraction of whole kidney mRNAs and real-time PCR are detailed in the Supplementary Methods section. The amount of PCR product in each sample was calculated as the percentage of a RNA standard curve established with serial dilutions of a mouse whole kidney cDNA stock solution,[46,47] then

revised according to the amount of PCR product for mRNA of the housekeeping *RPL26* gene. The list of all specific primers for mouse genes is given in Table S3.

Immunohistochemistry. Immunohistochemistry was performed on kidney slices using the procedure detailed in Supplementary Methods section. Labeled slices were then examined using either a LSM710 laser scanning confocal microscope or an Axio Scan.Z1 digital slide scanner (Carl Zeiss, Marly Le Roy, France) and 16 bits-depth images were analyzed offline with the Zeiss Zen software. Intensity profiles (see the Results section) were drawn from the corresponding background-substracted signals, normalized to their maximum value over the measurement distance (20 µm).

Western blotting. Western blots were performed on protein extracts in the conditions detailed in Supplementary Methods section. Indirect protein detection was performed by either chemiluminescence using the Pierce™ ECL Western Blotting Substrate (ThermoFischer Scientific) or a iBright Western blot imager (ThermoFisher Scientific). The protein signal was quantified using the ImageJ freeware (NIH, Bethesda, USA) and routinely normalized on β-actin signal.

Measurement of membrane potential. The transmembrane potential difference in cells of microdissected proximal tubules was estimated using the non-invasive cell-attached zero current-clamp configuration as described by others investigators,[48,49] in the conditions detailed in the Supplementary Methods section. The accuracy of this method increases with the resistance ratio $R_{Seal}/R_{Patch+Cell,}$[49] and low R_{Seal} values may lead to significant membrane potential underestimation. Nevertheless, membrane potential estimates in a given condition were independent of the 1.1-12 GΩ range of R_{Seal} values obtained in this study (Supplementary Figure S6). Because the prolonged zero current-clamp condition almost systematically altered patch

seals resistance and prevented reliable paired V_m measurements in the presence of Ba^{2+}, a separate series of measurements was performed with the blocker continuously present in the bath solution.

Measurements of intracellular pH in proximal cells. Intracellular pH of isolated proximal tubules microperfused *in vitro* was assessed by fluorescence imaging microscopy using 2′,7′-Bis-(2-Carboxyethyl)-5-(and-6)-carboxyfluorescein (BCECF, ThermoFisher Scientific), as detailed in the Supplementary Methods section.

Rate constants (k) of pH_i changes were determined by an iterative least-square curve-fitting procedure used to fit the data to a single exponential equation of the form

$$Y = Yo + A * e^{kt}$$

as described by other investigators.[26]

Statistical analyses. Results are given as means ± SEM for the indicated number of experiments or as individual values. Statistical significance of difference between means was evaluated by bilateral Student's t test using Systat Sigmastat 3.5 software (Ritme Informatique, Paris, France) with significance determined at a P value < 0.05.

DISCLOSURE

All the authors declared no competing interests.

REFERENCES

1. Kraut JA, Madias NE. Consequences and therapy of the metabolic acidosis of chronic kidney disease. *Pediatr. Nephrol.* 2011; **26**: 19–28.

2. Vallet M, Metzger M, Haymann J-P *et al.* Urinary ammonia and long-term outcomes in chronic kidney disease. *Kidney Int.* 2015; **88**: 137–145.

3. Haque SK, Ariceta G, Batlle D. Proximal renal tubular acidosis: a not so rare disorder of multiple etiologies. *Nephrol. Dial. Transplant. Off. Publ. Eur. Dial. Transpl. Assoc. - Eur. Ren. Assoc.* 2012; **27**: 4273–4287.

4. Handlogten ME, Osis G, Lee H-W *et al.* NBCe1 expression is required for normal renal ammonia metabolism. *Am. J. Physiol. Renal Physiol.* 2015; **309**: F658-666.

5. Lee H-W, Osis G, Harris AN *et al.* NBCe1-A Regulates Proximal Tubule Ammonia Metabolism under Basal Conditions and in Response to Metabolic Acidosis. *J. Am. Soc. Nephrol. JASN* 2018; **29**: 1182–1197.

6. Gawenis LR, Bradford EM, Prasad V *et al.* Colonic anion secretory defects and metabolic acidosis in mice lacking the NBC1 Na+/HCO3- cotransporter. *J. Biol. Chem.* 2007; **282**: 9042–9052.

7. Katzir Z, Dinour D, Reznik-Wolf H *et al.* Familial pure proximal renal tubular acidosis--a clinical and genetic study. *Nephrol. Dial. Transplant. Off. Publ. Eur. Dial. Transpl. Assoc. - Eur. Ren. Assoc.* 2008; **23**: 1211–1215.

8. Nagami GT. Effect of bath and luminal potassium concentration on ammonia production and secretion by mouse proximal tubules perfused in vitro. *J. Clin. Invest.* 1990; **86**: 32–39.

9. Völkl H, Lang F. Electrophysiology of ammonia transport in renal straight proximal tubules. *Kidney Int.* 1991; **40**: 1082–1089.

10. Hebert SC, Desir G, Giebisch G *et al.* Molecular diversity and regulation of renal potassium channels. *Physiol. Rev.* 2005; **85**: 319–371.

11. He W, Liu W, Chew CS *et al.* Acid secretion-associated translocation of KCNJ15 in gastric parietal cells. *Am. J. Physiol. Gastrointest. Liver Physiol.* 2011; **301**: G591-600.

12. Hill CE, Briggs MM, Liu J *et al.* Cloning, expression, and localization of a rat hepatocyte inwardly rectifying potassium channel. *Am. J. Physiol. Gastrointest. Liver Physiol.* 2002; **282**: G233-240.

13. Hibino H, Fujita A, Iwai K *et al.* Differential assembly of inwardly rectifying K+ channel subunits, Kir4.1 and Kir5.1, in brain astrocytes. *J. Biol. Chem.* 2004; **279**: 44065–44073.

14. Chabardès-Garonne D, Mejéan A, Aude J-C *et al.* A panoramic view of gene expression in the human kidney. *Proc. Natl. Acad. Sci. U. S. A.* 2003; **100**: 13710–13715.

15. Weiner ID, Verlander JW. Ammonia transport in the kidney by Rhesus glycoproteins. *Am. J. Physiol. Renal Physiol.* 2014; **306**: F1107-1120.

16. Weiner ID, Verlander JW. Role of NH3 and NH4+ transporters in renal acid-base transport. *Am. J. Physiol. - Ren. Physiol.* 2011; **300**: F11–F23.

17. Moret C, Dave MH, Schulz N *et al.* Regulation of renal amino acid transporters during metabolic acidosis. *Am. J. Physiol. Renal Physiol.* 2007; **292**: F555-566.

18. Schoolwerth AC, deBoer PA, Moorman AF *et al.* Changes in mRNAs for enzymes of glutamine metabolism in kidney and liver during ammonium chloride acidosis. *Am. J. Physiol.* 1994; **267**: F400-406.

19. Halperin ML, Kamel KS, Ethier JH *et al.* What is the underlying defect in patients with isolated, proximal renal tubular acidosis? *Am. J. Nephrol.* 1989; **9**: 265–268.

20. Matsumura Y, Aoki S, Fujimoto M. Regulatory mechanism of cell pH in the renal proximal tubule of bullfrog nephron. *Jpn. J. Physiol.* 1985; **35**: 741–763.

21. Warth R, Barrière H, Meneton P *et al.* Proximal renal tubular acidosis in TASK2 K+ channel-deficient mice reveals a mechanism for stabilizing bicarbonate transport. *Proc. Natl. Acad. Sci. U. S. A.* 2004; **101**: 8215–8220.

22. Wang WH, Wang Y, Silbernagl S *et al.* Fused cells of frog proximal tubule: II. Voltage-dependent intracellular pH. *J. Membr. Biol.* 1988; **101**: 259–265.

23. Alpern RJ. Mechanism of basolateral membrane H+/OH-/HCO-3 transport in the rat proximal convoluted tubule. A sodium-coupled electrogenic process. *J. Gen. Physiol.* 1985; **86**: 613–636.

24. Völkl H, Greger R, Lang F. Potassium conductance in straight proximal tubule cells of the mouse. Effect of barium, verapamil and quinidine. *Biochim. Biophys. Acta* 1987; **900**: 275–281.

25. Vallon V, Grahammer F, Richter K *et al.* Role of KCNE1-Dependent K+ Fluxes in Mouse Proximal Tubule. *J. Am. Soc. Nephrol.* 2001; **12**: 2003–2011.

26. Boron WF, Boulpaep EL. Intracellular pH regulation in the renal proximal tubule of the salamander. Basolateral HCO3- transport. *J. Gen. Physiol.* 1983; **81**: 53–94.

27. Yoshitomi K, Burckhardt BC, Frömter E. Rheogenic sodium-bicarbonate cotransport in the peritubular cell membrane of rat renal proximal tubule. *Pflugers Arch.* 1985; **405**: 360–366.

28. Völkl H, Geibel J, Greger R *et al.* Effects of ouabain and temperature on cell membrane potentials in isolated perfused straight proximal tubules of the mouse kidney. *Pflugers Arch.* 1986; **407**: 252–257.

29. Edvinsson JM, Shah AJ, Palmer LG. Kir4.1 K+ channels are regulated by external cations. *Channels* 2011; **5**: 269–279.

30. Weinstein AM. Ammonia transport in a mathematical model of rat proximal tubule. *Am. J. Physiol.-Ren. Physiol.* 1994; **267**: F237–F248.

31. Kurtz I, Balaban RS. Ammonium as a substrate for Na+-K+-ATPase in rabbit proximal tubules. *Am. J. Physiol.* 1986; **250**: F497-502.

32. Garvin JL, Burg MB, Knepper MA. Ammonium replaces potassium in supporting sodium transport by the Na-K-ATPase of renal proximal straight tubules. *Am. J. Physiol.* 1985; **249**: F785-788.

33. Weiner ID, Verlander JW. Renal ammonia metabolism and transport., Renal Ammonia Metabolism and Transport. *Compr. Physiol. Compr. Physiol.* 2013; **3, 3**: 201, 201–220.

34. Chaudhry FA, Reimer RJ, Krizaj D *et al.* Molecular analysis of system N suggests novel physiological roles in nitrogen metabolism and synaptic transmission. *Cell* 1999; **99**: 769–780.

35. Ambühl PM, Amemiya M, Danczkay M *et al.* Chronic metabolic acidosis increases NHE3 protein abundance in rat kidney. *Am. J. Physiol.* 1996; **271**: F917-925.

36. Laghmani K, Borensztein P, Ambühl P *et al.* Chronic metabolic acidosis enhances NHE-3 protein abundance and transport activity in the rat thick ascending limb by increasing NHE-3 mRNA. *J. Clin. Invest.* 1997; **99**: 24–30.

37. Soleimani M, Grassi SM, Aronson PS. Stoichiometry of Na+-HCO-3 cotransport in basolateral membrane vesicles isolated from rabbit renal cortex. *J. Clin. Invest.* 1987; **79**: 1276–1280.

38. Sasaki S, Berry CA. Mechanism of bicarbonate exit across basolateral membrane of the rabbit proximal convoluted tubule. *Am. J. Physiol.* 1984; **246**: F889-896.

39. Horita S, Yamada H, Inatomi J *et al.* Functional analysis of NBC1 mutants associated with proximal renal tubular acidosis and ocular abnormalities. *J. Am. Soc. Nephrol. JASN* 2005; **16**: 2270–2278.

40. Brenes LG, Sanchez MI. Impaired urinary ammonium excretion in patients with isolated proximal renal tubular acidosis. *J. Am. Soc. Nephrol. JASN* 1993; **4**: 1073–1078.

41. Igarashi T, Sekine T, Inatomi J *et al.* Unraveling the Molecular Pathogenesis of Isolated Proximal Renal Tubular Acidosis. *J. Am. Soc. Nephrol.* 2002; **13**: 2171–2177.

42. Lemann J, Adams ND, Wilz DR *et al.* Acid and mineral balances and bone in familial proximal renal tubular acidosis. *Kidney Int.* 2000; **58**: 1267–1277.

43. Welling PA. Roles and Regulation of Renal K Channels. *Annu. Rev. Physiol.* 2016; **78**: 415–435.

44. Karet FE. Mechanisms in hyperkalemic renal tubular acidosis. *J. Am. Soc. Nephrol. JASN* 2009; **20**: 251–254.

45. Paulais M, Bloch-Faure M, Picard N *et al.* Renal phenotype in mice lacking the Kir5.1 (Kcnj16) K+ channel subunit contrasts with that observed in SeSAME/EAST syndrome. *Proc. Natl. Acad. Sci. U. S. A.* 2011; **108**: 10361–10366.

46. Lachheb S, Cluzeaud F, Bens M *et al.* Kir4.1/Kir5.1 channel forms the major K+ channel in the basolateral membrane of mouse renal collecting duct principal cells. *Am. J. Physiol. Renal Physiol.* 2008; **294**: F1398-1407.

47. Paulais M, Lachheb S, Teulon J. A Na+- and Cl- -activated K+ channel in the thick ascending limb of mouse kidney. *J. Gen. Physiol.* 2006; **127**: 205–215.

48. Mason MJ, Simpson AK, Mahaut-Smith MP *et al.* The interpretation of current-clamp recordings in the cell-attached patch-clamp configuration. *Biophys. J.* 2005; **88**: 739–750.

49. Perkins KL. Cell-attached voltage-clamp and current-clamp recording and stimulation techniques in brain slices. *J. Neurosci. Methods* 2006; **154**: 1–18.

ACKNOWLEDGMENTS

Y.B. and L.P. hold PhD fellowships from the Ministère de l'Enseignement Supérieur et de la Recherche. We thank Nathalie Reveilleau and Stéphanie Baron (Unité d'explorations fonctionnelles métaboliques et rénales *in vivo*, Hôpital Européen Georges Pompidou, Paris, France) for their expert technical assistance in the measurement of urine NH_4^+ and titratable acidity in mice, and Dr Geneviève Escher (Department of Nephrology and Hypertension Inselspital, Universitätsklinik für Nephrologie und Hypertonie, Bern, Switzerland) for aldosterone measurements. We are also grateful to Christophe Klein and Kévin Garbin (Centre d'Imagerie Cellulaire et de Cytométrie, Centre de Recherche des Cordeliers, Paris, France) for their help with microscopy resources, and to the members of the Centre d'Explorations Fonctionnelles and of the Centre de Génotypage et de Biochimie (Centre de Recherche des Cordeliers, Paris, France) for taking care of mice and genotyping.

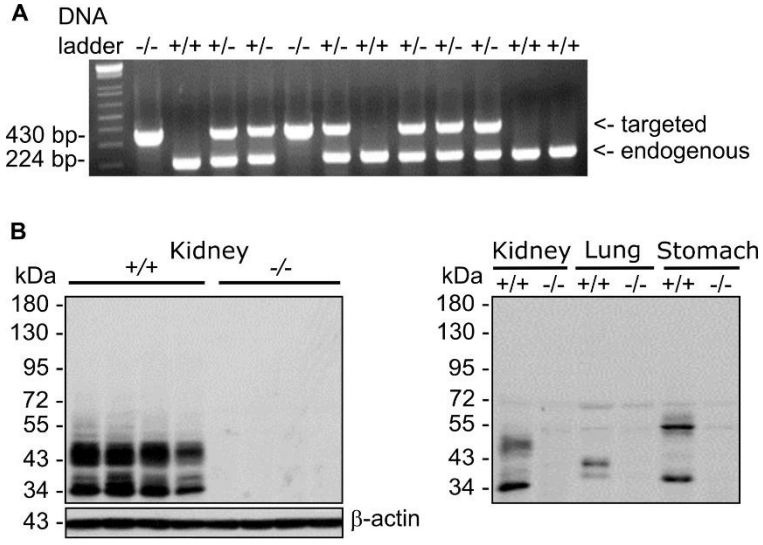

Figure 1. Mice with deletion of *Kcnj15* and Kir4.2 tissular expression. (a) Multiplex polymerase chain reaction analysis of tail biopsy cDNA from the offspring of a heterozygous mating identified 224-bp and 430-bp amplicons from endogenous and targeted alleles, respectively. (**b**) Western blotting for Kir4.2 in whole tissue extracts from *Kcnj15*$^{+/+}$ (+/+) and *Kcnj15*$^{-/-}$ (-/-) mice. In the right panel, the tissues originated from the same mouse of the corresponding genotype. Either β-actin (left panel) or Ponceau-S staining (right panel; not shown) was used as the loading control.

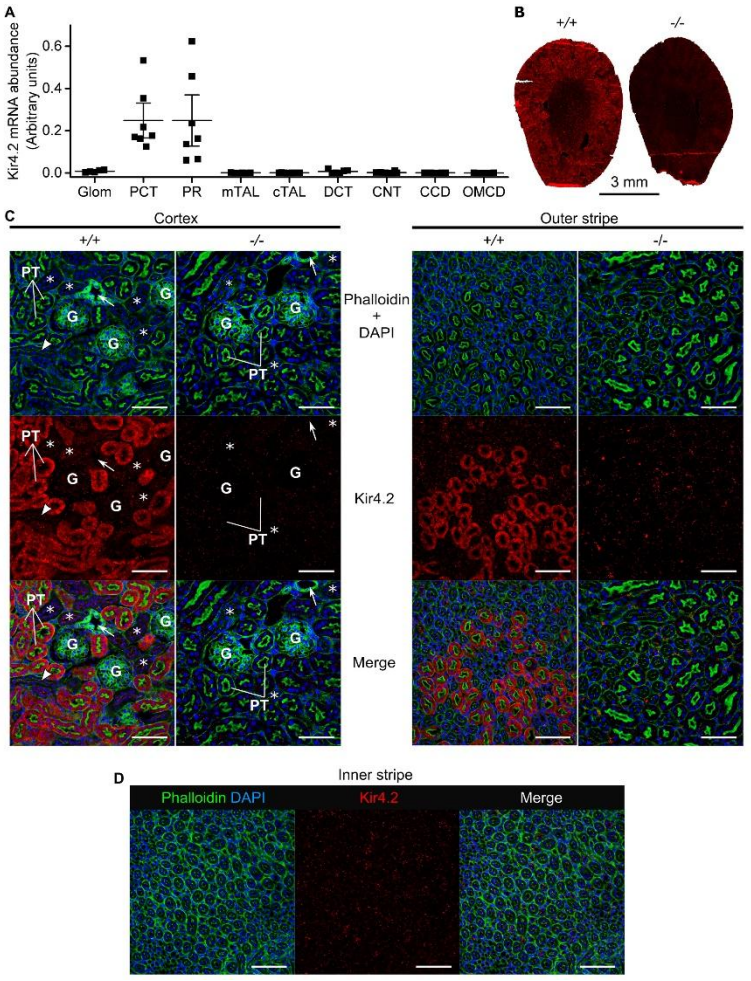

Figure 2. Renal Kir4.2 cellular distribution in mice. (**a**) Kir4.2 mRNA distribution along the mouse nephron. (**b**) *Kcnj15*$^{+/+}$ (+/+) and *Kcnj15*$^{-/-}$ (-/-) mice whole kidneys cross sections probed with the anti-Kir4.2 antibody. (**c** and **d**) Confocal images of cortex (c, left), outer stripe of the outer medulla (C, right) and inner stripe of the outer medulla (d) regions of mice kidneys stained with Alexa Fluor® 488 phalloidin (green) and DAPI (blue), and probed with anti-Kir4.2 antibody (red). In (**d**), only images of a *Kcnj15*$^{+/+}$ mouse kidney are shown. Bars = 70 µm. * : Distal convoluted tubule (DCT); arrowhead : connecting tubule:cortical collecting duct (CNT/CCD); arrow : blood vessel. CNT, connecting tubule; cTAL, cortical thick ascending limbs; G : glomerulus. Glom, glomerulus; mTAL, medullary thick ascending limbs. OMCD, outer medullary collecting duct. PCT, proximal convoluted tubule; PR, *pars recta*; PT, proximal tubule.

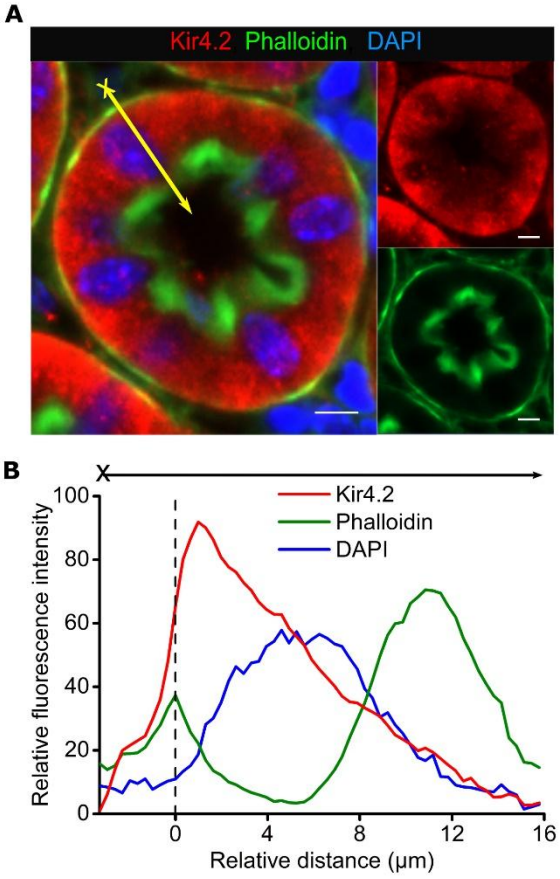

Figure 3. Subcellular localization of Kir4.2. Fluorescence images (**a**) and associate intensity profiles (**b**) of cortical proximal tubular cells of *Kcnj15*$^{+/+}$ mice labeled with 4',6-diamidino-2-phenylindole (DAPI; blue) and Alexa Fluor 488 phalloidin (green) and costained with the anti-Kir4.2 antibody (red). The profile of each fluorescence channel was established along the line represented as an arrow, taking the maximum phalloidin fluorescence level at the basal pole (dotted line) as the origin. Traces are means of measurements on 13 cells. Bars = 5 μm.

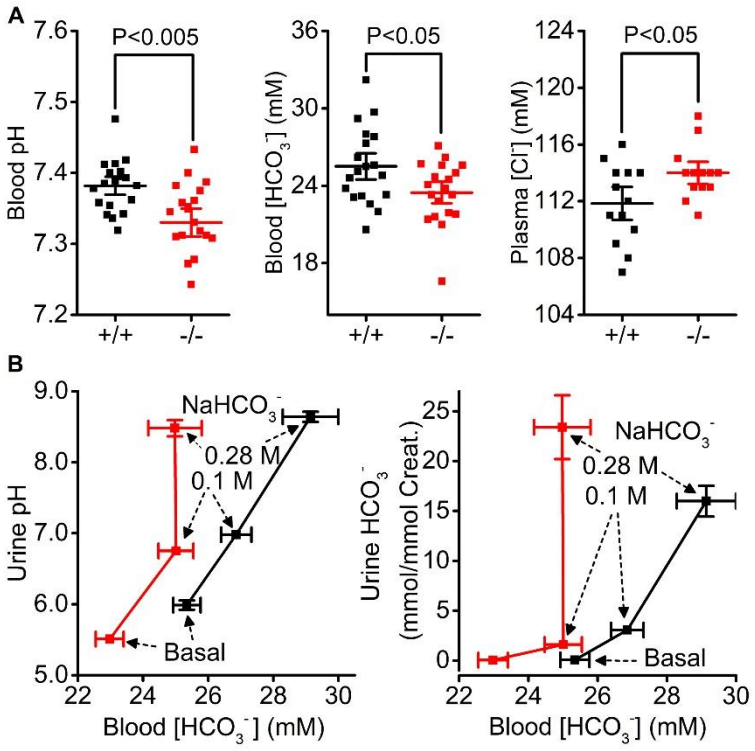

Figure 4. Acid-base status and HCO_3^- handling in mice with the deletion of *Kcnj15*. (**a**) Basal blood and plasma parameters of *Kcnj15*$^{+/+}$ (+/+, black squares) and *Kcnj15*$^{-/-}$ (-/-, red squares) mice. (**b**) Urine pH and HCO_3^- contents in *Kcnj15*$^{+/+}$ (black squares) and *Kcnj15*$^{-/-}$ (red squares) mice as a function of blood HCO_3^- content, under basal condition and after 1 day of the indicated exogenous $NaHCO_3^-$ alkaline loads. Data are from 9 *Kcnj15*$^{+/+}$ and 12 *Kcnj15*$^{-/-}$ mice.

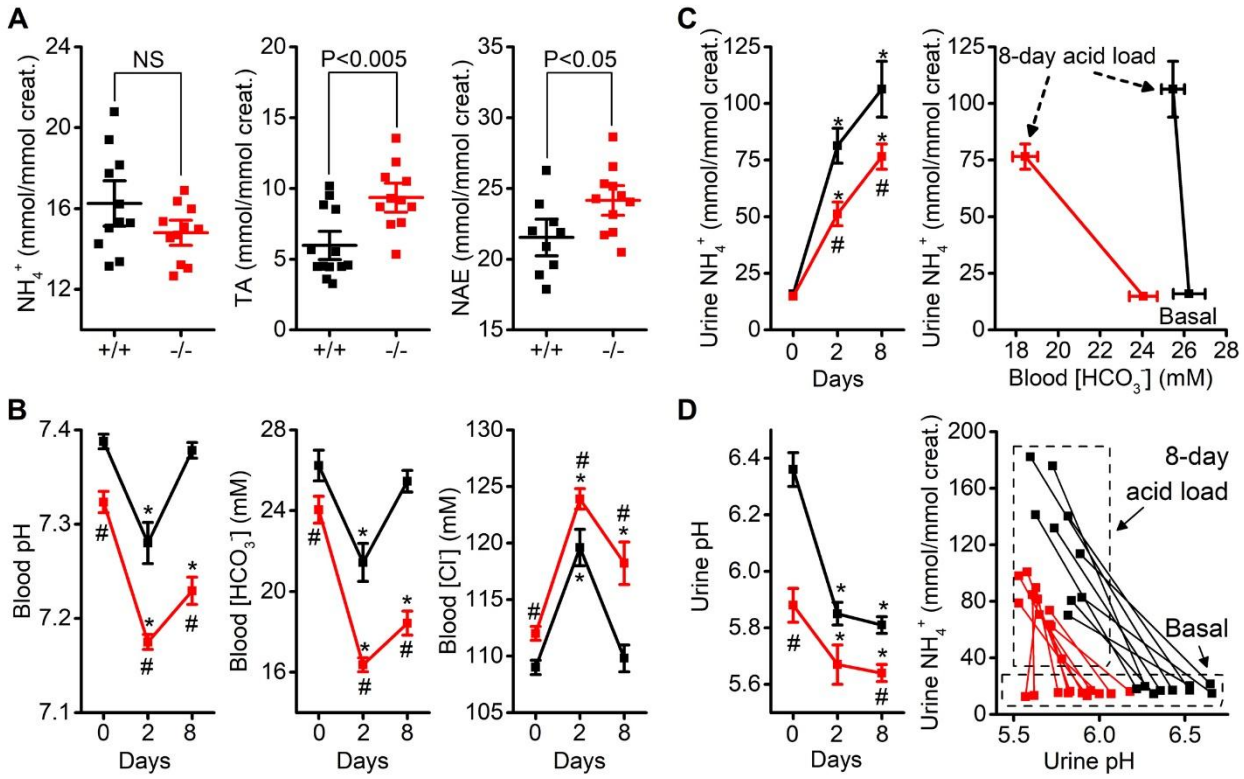

Figure 5. NH_4^+ excretion and distal acidification capabilities in mice with the deletion of *Kcnj15*. (**a**) Basal urine parameters of *Kcnj15*$^{+/+}$ (black squares) and *Kcnj15*$^{-/-}$ (red squares) mice. (**b-d**) Blood and urine parameters in 9 to 12 *Kcnj15*$^{+/+}$ (black squares) and 10-11 *Kcnj15*$^{-/-}$ (red squares) mice challenged with an oral 0.28 M NH_4Cl acid load for 8 days. * $P < 0.05$ versus day 0 and # $P < 0.05$ versus *Kcnj15*$^{+/+}$ mice. Creat., creatinine; NAE, net acid excretion. NS, no significant difference. TA, titratable acidity.

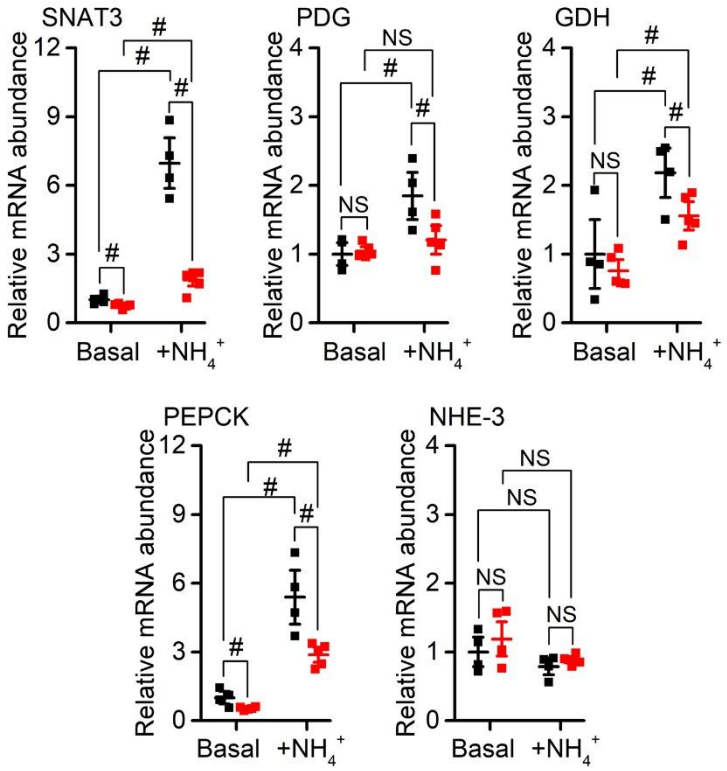

Figure 6. Expression of mRNA of proteins involved in proximal ammonia metabolism in mice with the deletion of *Kcnj15*. Renal expressions of mRNAs for the systen N1 Na^+ and H^+-coupled glutamine transporter (SNAT3), the ammoniagenic enzymes phosphate-dependent glutaminase (PDG), glutamate dehydrogenase (GDH), and phosphoenolpyruvate kinase (PEPCK), and the NH_4^+ exit pathway Na^+/H^+ exchanger 3 (NHE-3) in *Kcnj15*$^{+/+}$ (black squares) and *Kcnj15*$^{-/-}$ (red squares) mice, under basal (n = 4 and 5 mice, respectively) and NH_4Cl-induced acid load ($+NH_4$; n = 4 and 6 mice, respectively) conditions. Data were normalized to the respective basal expression in *Kcnj15*$^{+/+}$ mice. # $P < 0.05$. NS: no significant difference.

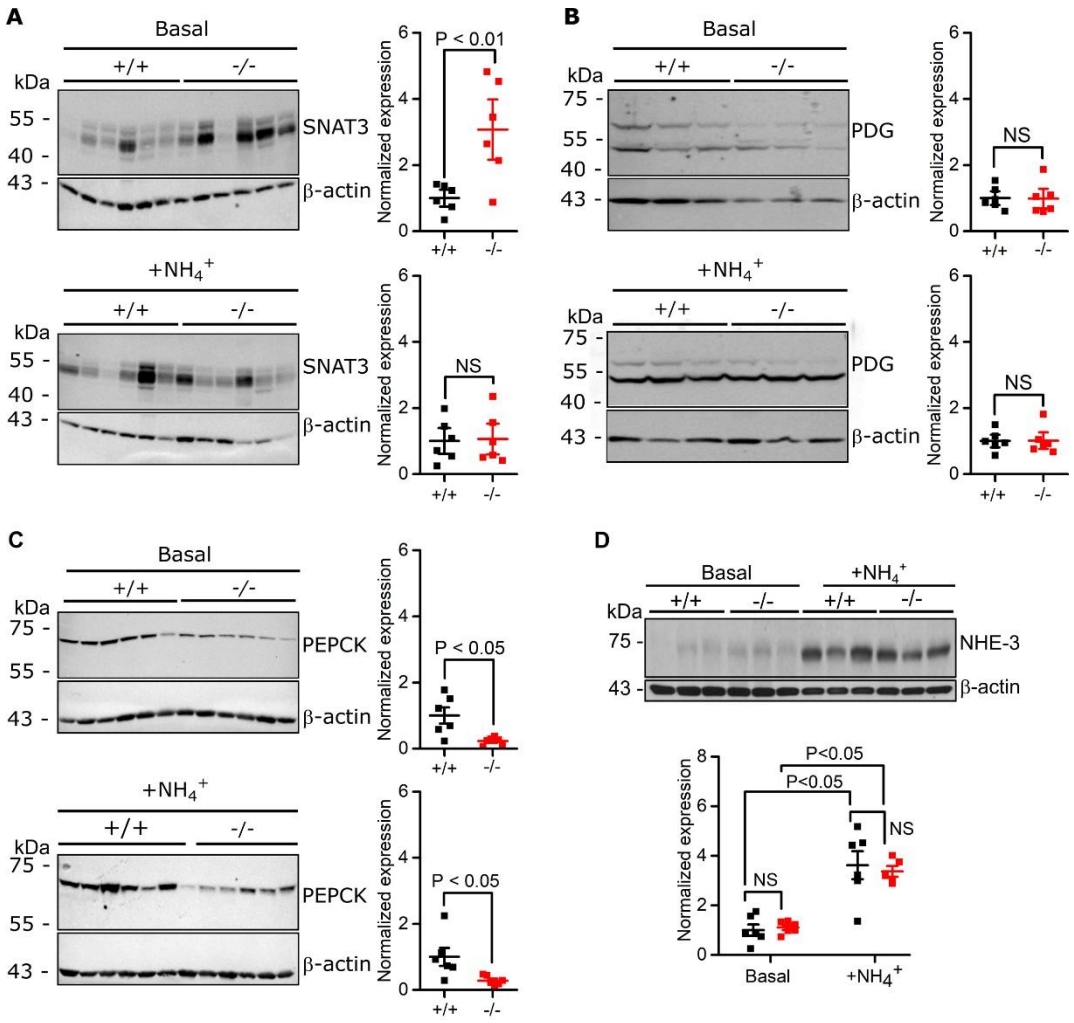

Figure 7. Peptide expression of proteins involved in proximal ammonia metabolism in mice with the deletion of *Kcnj15*. Renal system N1 Na^+ and H^+-coupled glutamine transporter (SNAT3) (**a**), phosphate-dependent glutaminase (PDG) (**b**), phosphoenolpyruvate carboxykinase (PEPCK) (**c**), and Na^+/H^+ exchanger 3 (NHE-3) peptide expressions in *Kcnj15*$^{+/+}$ (black squares) and *Kcnj15*$^{-/-}$ (red squares) mice, under basal and NH_4Cl-induced acid load (+NH4) conditions. Data shown in the graphs were normalized to their respective β-actin expression level and then to the respective basal expression in *Kcnj15*$^{+/+}$ mice, for 6 mice in each group and condition. NS: no significant difference.

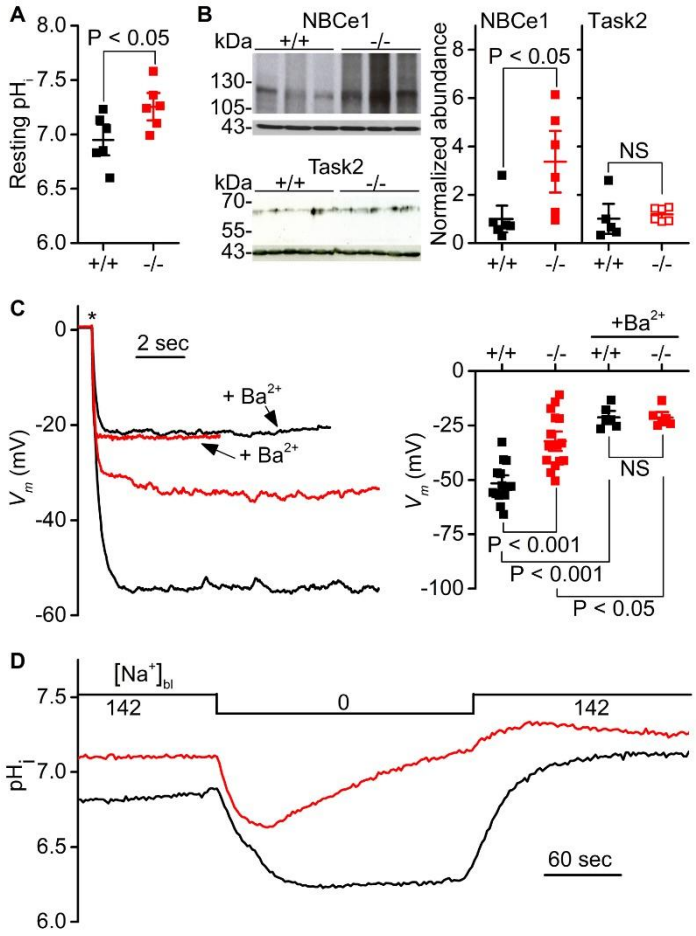

Figure 8. NBCe1 expression, membrane potential, and intracellular pH of proximal cells. (**a**) Summary of resting pH_i data for 6 *Kcnj15*$^{+/+}$ (+/+, black squares) and 6 *Kcnj15*$^{-/-}$ (-/-, red squares) mice. (**b**) Left panels : expression of the Na^+-coupled HCO_3^- cotransporter, isoform 1 (NBCe1) and of the TWIK-related acid-sensitive K^+ channel 2 (Task2) peptides in 3 *Kcnj15*$^{+/+}$ and 3 *Kcnj15*$^{-/-}$ mice. β-actin was used as the loading control. Right panel : quantification of NBCE1 and Task2 peptides expression after normalization to their respective expression in *Kcnj15*$^{+/+}$ mice. Data are from 6 *Kcnj15*$^{+/+}$ and 6 *Kcnj15*$^{-/-}$ mice. (**c**) Estimation of membrane potential (V_m) in *Kcnj15*$^{+/+}$ and *Kcnj15*$^{-/-}$ mice from cell-attached current-clamp recordings, in the presence (+Ba^{2+}) and absence of 1 mM Ba^{2+} in the bath. Left panel : typical V_m recordings for *Kcnj15*$^{+/+}$ (black line) and *Kcnj15*$^{-/-}$ (red line) mice. At the time indicated by the asterisk, the patch clamp

amplifier was switched from the *search mode* to the zero current-clamp (I0) mode, then V_m was measured at a steady state. Right panel : summary of V_m data for 14 *Kcnj15*$^{+/+}$ (black squares) and 16 *Kcnj15*$^{-/-}$ (red squares) mice. Data obtained in the absence of Ba^{2+} were normally distributed (Kolmogorov-Smirnov test : P = 0.17 for *Kcnj15*$^{+/+}$ mice and P = 0.18 for *Kcnj15*$^{-/-}$ mice). (**d**) Microfluorometric intracellular pH (pH_i) measurements in microperfused isolated proximal tubules. Left panel: pH_i recordings in *Kcnj15*$^{+/+}$ (black line) and *Kcnj15*$^{-/-}$ mice (red line), at the indicated basolateral Na^+ concentrations ($[Na^+]_{bl}$, in mM) and under constant (23 mM) bath HCO_3^- content. The luminal solution was the HCO_3^--containing and Na^+-free solution all throughout the measurement. NS, no significant difference between groups.

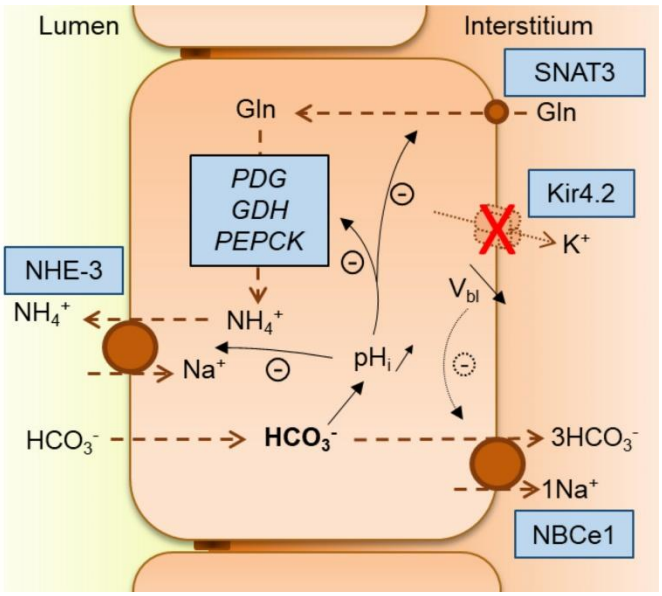

Figure 9. Proposed model for the defective ammonia metabolism in mice with the deletion of *Kcnj15*. The loss of Kir4.2 channels at the basolateral membrane decreases the basolateral membrane potential difference (V_{bl}) and the driving force for HCO_3^- exit by the rheogenic NBCe1. The resulting increase in intracellular HCO_3^- content increases pH_i and downregulates the expression of proteins involved in ammoniagenesis, glutamine (Gln) entry and NH_4^+ secretion. NBCe1, Na^+-coupled HCO_3^- cotransporter, isoform 1; NHE-3, Na^+/H^+ exchanger 3; PDG, phosphate-dependent glutaminase; PEPCK, phosphoenolpyruvate carboxykinase ; SNAT3, system N1 Na^+ and H^+-coupled glutamine transporter.

Parameter	*Kcnj15*$^{+/+}$	*Kcnj15*$^{-/-}$	Significance
Na^+, mM	148.8 ± 0.5 (22)	148.8 ± 0.5 (21)	NS
K^+, mM	5.7 ± 0.2 (9)	5.4 ± 0.3 (19)	NS
Ca^{2+}, mM	1.2 ± 0.01 (23)	1.3 ± 0.01 (21)	$P < 0.05$
Mg^{2+}, mM	0.9 ± 0.1 (13)	1 ± 0.1 (13)	NS
Phosphate, mM	2.8 ± 0.4 (13)	3.2 ± 0.2 (14)	NS
Glucose, mM	14.9 ± 1.2 (12)	14.9 ± 1.2 (13)	NS
Proteins, g/l	41.6 ± 1.2 (11)	40.8 ± 2.7 (11)	NS

Table 1. Plasma parameters of *Kcnj15*$^{+/+}$ and *Kcnj15*$^{-/-}$ mice maintained on a standard diet.

NS, no significant difference between groups.

Data are means ± SEM for the numbers of mice given in brackets.

Parameter	*Kcnj15*$^{+/+}$	*Kcnj15*$^{-/-}$	Significance
Uv (µl/g BW/ day)	72.9 ± 4.3 (22)	68.3 ± 7.3 (17)	NS
Osmolality (mOsm./Kg H_20)	2515 ± 180 (22)	2418 ± 131 (17)	NS
GFR (µl/min)	450 ± 35 (15)	387 ± 38 (14)	NS
FE-Na^+, %	0.33 ± 0.038 (9)	0.37 ± 0.04 (12)	NS
FE-K^+, %	14.5 ± 1.81 (10)	16.5 ± 2.01 (12)	NS
FE-Cl^-, %	0.4 ± 0.07 (7)	0.5 ± 0.06 (8)	NS
FE-Ca^{2+}, %	0.26 ± 0.0039 (14)	0.4 ± 0.05 (15)	< *P* 0.05
FE-Mg^{2+}, %	5.6 ± 0.61 (10)	6.1 ± 0.46 (12)	NS
FE-Proteins, %	0.03 ± 0.011 (9)	0.06 ± 0.02 (10)	NS
FE-Glucose, %	0.16 ± 0.025 (10)	0.16 ± 0.022 (11)	NS
FE-Phosphate, %	3.8 ± 0.88 (10)	3.9 ± 0.7 (12)	NS
Aldosterone, pg/g BW/day	100 ± 36 (6)	109 ± 40 (6)	NS

Table 2. Urine parameters of *Kcnj15*$^{+/+}$ and *Kcnj15*$^{-/-}$ mice maintained on a standard diet.

BW, body weight; FE, factional excretion; GFR, estimated glomerular filtration rate; NS, no significant difference between groups; Uv, urine volume.

Data are means ± SEM for the numbers of mice given in parentheses.

Bath Na^+ withdrawal						Bath Na^+ restoration					
Kcnj15$^{+/+}$			*Kcnj15*$^{-/-}$			*Kcnj15*$^{+/+}$			*Kcnj15*$^{-/-}$		
#	ΔpH_i	*k* (min^{-1})	#	ΔpH_i	*k* (min^{-1})	#	ΔpH_i	*k* (min^{-1})	#	ΔpH_i	*k* (min^{-1})
1	-0.34	-2.04	7	-0.41	-5.38	1	0.43	2.2	7	0.19	2.44
2	-1.26	-1.06	8	-0.46	-5.27	2	1.77	1.24	8	0.09	nd
3	-0.4	-5.75	9	-0.24	-15	3	0.72	2.76	9	0.45	2.64
4	-0.42	-2.52	10	-0.8	-0.92	4	0.58	2.96	10	0.91	2.15
5	-0.6	-2.01	11	-0.6	-1.48	5	0.84	1.96	11	0.77	1.41
6	-0.17	-3.94				6	0.15	4.4			
	0.53 ± 0.171	-2.88 ± 0.755		0.5 ± 0.105	-5.61 ± 2.821		0.75 ± 0.248	2.59 ± 0.483		0.48 ± 0.178	2.16 ± 0.312

Table 3. Kinetics parameters of the changes in pH_i of proximal cells induced by bath Na^+ withdrawal and restoration.

nd : not determined; pH_i, intracellular pH.

The tubules initially were bathed in the bath solution containing Na^+ and then exposed to Na^+-free (Bath Na^+ withdrawal) then back to Na^+-containing (Bath Na^+ restoration) bath solutions, under constant (23 mM) bath HCO_3^- content. The luminal solution was the HCO_3^--containing and Na^+-free solution all throughout the measurement. ΔpH_i is the amplitude of the change in pH_i induced by the indicated bath Na^+ manipulation and *k* is the rate constant. Individual values for each tubule (#) are reported and the means ± SEM are given in the last line. None of the means for *Kcnj*15$^{-/-}$ mice is statiscally different from the corresponding mean in *Kcnj15*$^{+/+}$ mice.

SUPPLEMENTARY MATERIAL

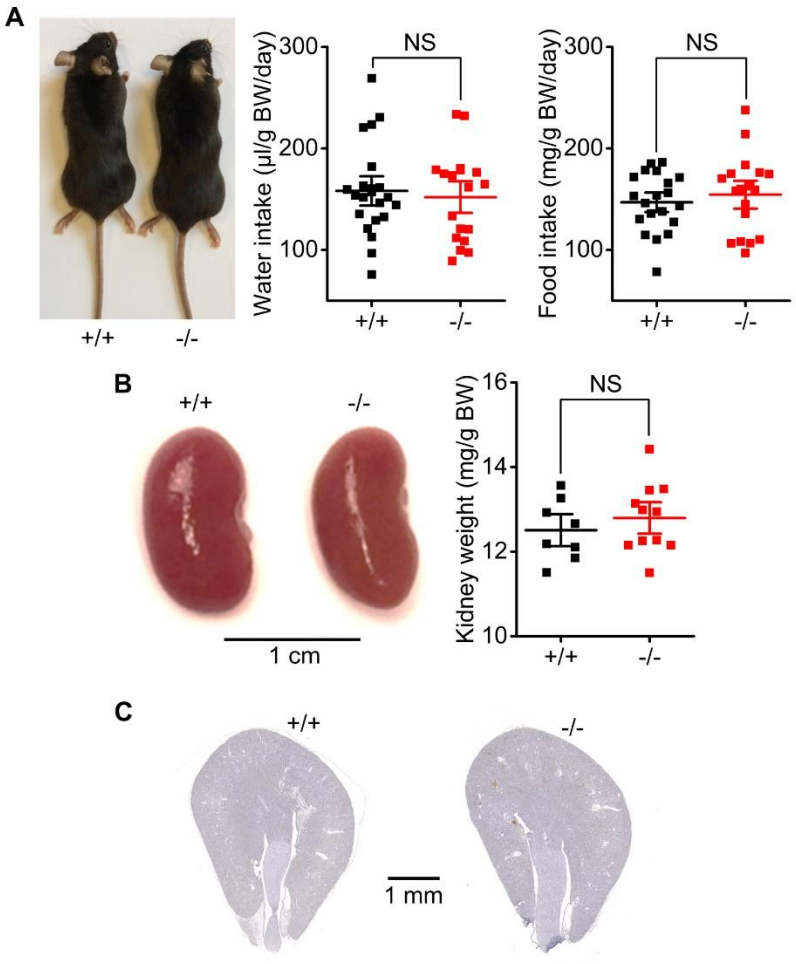

Figure S1. **Gross external appearance, food and water inputs, and renal anatomy in Kir4.2-deleted mice.** (**A**) Physical appearance of adult age-matched male *Kcnj15*$^{+/+}$ (+/+) and *Kcnj15*$^{-/-}$ (-/-) mice, and food (left panel) and water (right panel) intakes of 22 +/+ (■) and 18 -/- (■) mice. (**B**) Left panel: photographs of left kidneys. Right panel: kidneys weight of 11 +/+ (■) and 8 -/- (■) mice. (**C**) Hematoxylin–eosin stained kidney slices. NS: no significant difference.

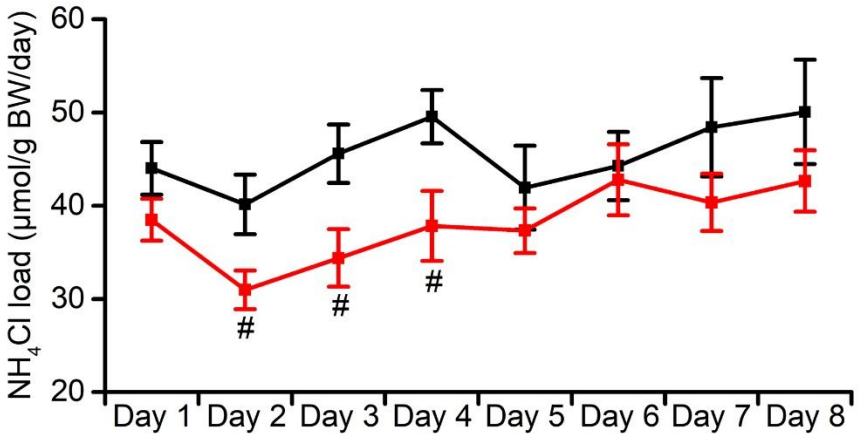

Figure S2. Evolution of the daily NH_4Cl load. 9-12 *Kcnj15*$^{+/+}$ (■) and 10-11 *Kcnj15*$^{-/-}$ mice (■) were challenged with 0.28 M NH_4Cl in the drinking water. BW : body weight. # $P < 0.05$.

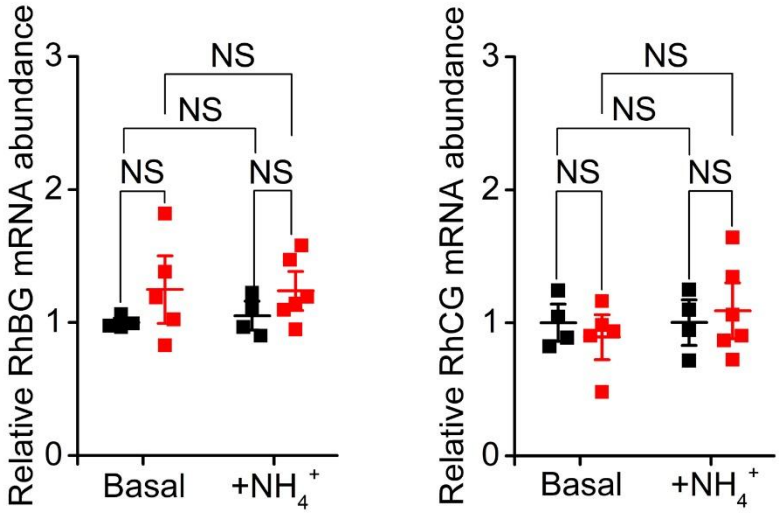

Figure S3. *Kcnj15*$^{-/-}$ mice display normal RhBG and RhCG mRNA expression. RhBG and RhCG mRNA expression in whole kidneys of 4 *Kcnj15*$^{+/+}$ (■) and 5-6 *Kcnj15*$^{-/-}$ (■) mice were measured under basal and exogenous acid load (+NH_4) conditions. NS: no significant difference.

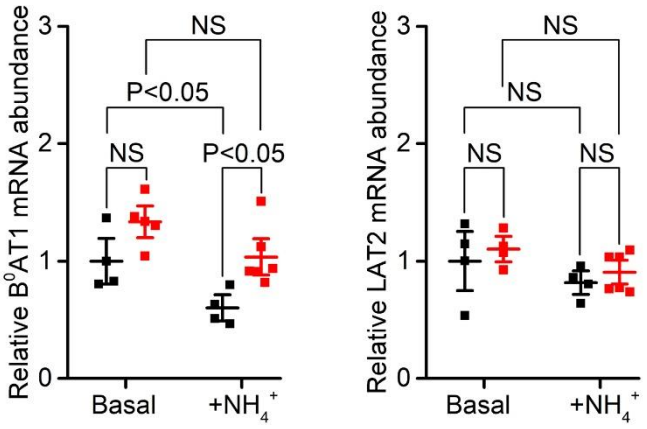

Figure S4. B^0AT1 and LAT2 gluatmine transporter mRNA expression. B^0AT1 (left panel) and LAT2 (right panel) mRNA expressions were measured by RT -qPCR from whole kidney mRNA of 4 *Kcnj15*$^{+/+}$ (■) and 5 *Kcnj15*$^{-/-}$ (■) mice under basal and exogenous acid load ($+NH_4$) conditions. NS: no significant difference.

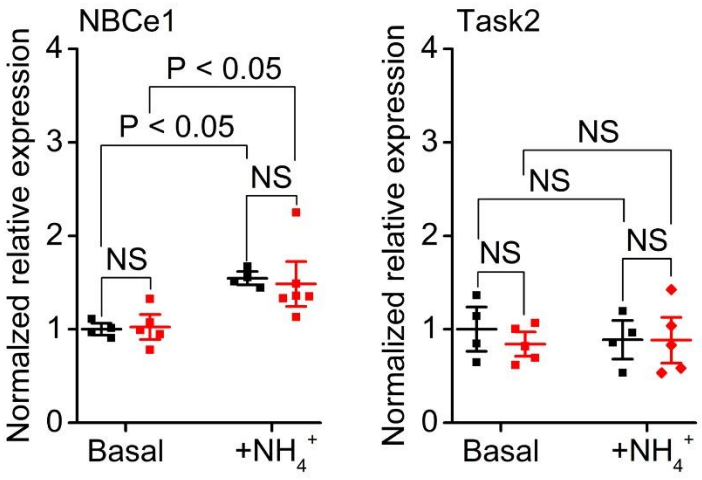

Figure S5. **Renal NBCe1 and Task2 mRNA expression**. NBCe1 (left panel) and TASK2 (right panel) mRNA expression was measured by RT-qPCR from whole kidney mRNA of 4 *Kcnj15*$^{+/+}$ (■) and 5 *Kcnj15*$^{-/-}$ (■) mice under basal and exogenous acid load (+NH_4) conditions. NS: no significant difference.

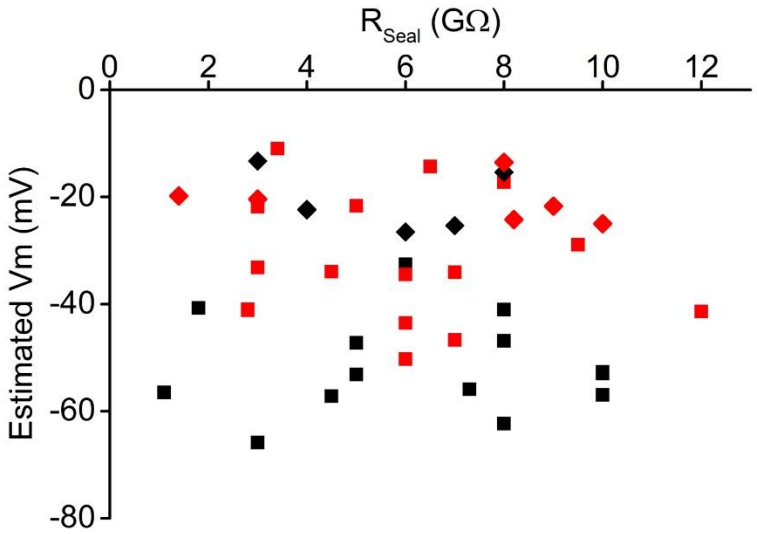

Figure S6. Estimation of resting membrane potential of proximal cells. Membrane potential (Vm) values estimated in *Kcnj15*$^{+/+}$ and *Kcnj15*$^{-/-}$ mice, in the presence (♦ and ♦, respectively) and absence (■ and ■, respectively) of 1 mM barium, are reported as a function of seal resistance (R_{Seal}).

Parameter	100 mM $NaHCO_3$ load			280 mM $NaHCO_3$ load		
	Kcnj15$^{+/+}$	*Kcnj15*$^{-/-}$	*P* Value	*Kcnj15*$^{+/+}$	*Kcnj15*$^{-/-}$	*P* Value
Body weight (g)	28 ± 0.2	27 ± 0.2	NS	27 ± 0.7	25 ± 1.1	NS
Water intake (µl/g BW/day)	160 ± 2.5	176 ± 3.6	NS	230 ± 17	238 ± 17.1	NS
Blood pH	7.39 ± 0.002	7.36 ± 0.002	<0.005	7.41 ± 0.012	7.36 ± 0.012	<0.01
Plasma [Cl^-] (mM)	113.6 ± 0.12	115.3 ± 0.12	<0.05	111 ± 1.23	114.2 ± 0.96	<0.05
Plasma [Ca^{2+}] (mM)	1.19 ± 0.002	1.23 ± 0.002	NS	1.14 ± 0.015	1.19 ± 0.011	<0.05
Uv (µl/g BW/ day)	44 ± 1.1	41 ± 1.3	NS	44 ± 5.9	74 ± 7.2	<0.005
Urine Ca^{2+} (mmol/mmol creat.)	0.2 ± 0.06	0.22 ± 0.003	NS	0.08 ± 0.006	0.12 ± 0.014	<0.01
HCO_3^- filtered load (mmol/g BW/day)	0.29 ± 0.017	0.25 ± 0.014	NS	0.5 ± 0.05	0.42 ± 0.038	NS

Table S1. Physiologic parameters of *Kcnj15*$^{+/+}$ and *Kcnj15*$^{-/-}$ mice after an alkaline load. Parameters were measured after a 24-hour oral 0.1 M or 0.28 M $NaHCO_3$-induced alkaline load. Results are from 6-18 *Kcnj15*$^{+/+}$ mice and 8-18 *Kcnj15*$^{-/-}$ mice. Uv : urine volume. BW : body weight. *NS* : no significant difference.

	Kcnj15$^{+/+}$			*Kcnj15*$^{-/-}$		
	Day 0	Day 2	Day 8	Day 0	Day 2	Day 8
Total body weight (g)	24.7 ± 1	24.5 ± 1	24.9 ± 1.2	24.6 ± 0.9	24.3 ± 0.9	24.5 ± 0.9
Water intake (µl/g BW/day)	145 ± 11	143 ± 11	179 ± 20*	150 ± 12	111 ± 7*†	152 ± 12
Uv (µl/g BW/ day)	71.6 ± 6.8	50.4 ± 5.8*	79.9 ± 8	77.6 ± 10.9	37 ± 4.6*	71 ± 3.4
Osmolality (mOsm/kg H_20)	2462 ± 252	3602 ± 251*	2924 ± 212	2461 ± 184	4348 ± 315*	3506 ± 185*
Na^+ (mmol/mmol creat.)	60.5 ± 4.6	61.8 ± 3.7	68.3 ± 6.4*	58.9 ± 7.2	59.2 ± 3.9	66 ± 4.6*
K^+ (mmol/mmol creat.)	57.2 ± 5.3	63.5 ± 6.8	66.6 ± 4.1*	55.2 ± 4.8	55.5 ± 5.9	66.8 ± 4.3*
Cl^- (mmol/mmol creat.)	61.3 ± 2.5	162.4 ± 9.9*	216.7 ± 19.4*	58.5 ± 3.4	126.4 ± 7.6*†	185 ± 7.7*
Ca^{2+} (mmol/mmol creat.)	0.29 ± 0.03	0.62 ± 0.11*	0.83 ± 0.15*	0.54 ± 0.09†	1.37 ± 0.25*†	2.84 ± 0.43*†
Mg^{2+} (mmol/mmol creat.)	5 ± 0.3	4.9 ± 0.5	6.3 ± 0.3*	5.4 ± 0.4	4.6 ± 0.2*	6.1 ± 0.3*
Phosphate (mmol/mmol creat.)	12 ± 0.9	9.8 ± 0.8	10.7 ± 1.3	13.8 ± 1.1	12.2 ± 1.1	14.7 ± 1.2*†
Proteins (g/mmol creat.)	0.99 ± 0.34	0.63 ± 0.19*	0.6 ± 0.17	1.05 ± 0.38	0.71 ± 0.19	0.53 ± 0.08
Glucose (mmol/mmol creat.)	0.43 ± 0.04	0.59 ± 0.09*	0.75 ± 0.12*	0.41 ± 0.04	0.75 ± 0.11*	0.91 ± 0.15*

Table S2. Clinical and urine parameters of *Kcnj15*$^{+/+}$ and *Kcnj15*$^{-/-}$ mice under basal and acid-loading conditions. Parameters were mesured before (Day 0) and after 2 or 8 days of an oral 0.28 M NH_4Cl-induced acid load. Results are from 12 *Kcnj15*$^{+/+}$ and 11 *Kcnj15*$^{-/-}$ mice. Uv : urine volume. BW : body weight. * $P < 0.05$ *vs* Day 0 (paired Student's t test), † $P < 0.05$ *vs* *Kcnj15*$^{+/+}$ mice at the given day (unpaired bilateral Student's t test).

RT-qPCR : targeted cDNA (*gene*)	Forward primer	Reverse primer
Kir4.2 (*Kcnj15*)	5'-GCAGGCCATAGCAGAG-3'	5'-GTGAGCTTGTATCGCCA-3'
NHE-3 (*Slc9a3*)	5'-TCCCTGGCCTTCATTCG-3'	5'-GTCACCCACCACACACT-3'
Task2 (*Kcnk5*)	5'-CTTGCACTAAGCTAGACATT-3'	5'-CTTCTGCACTTTCGGG-3'
NBCE1 (*Slc4a4*)	TCCGACAAATCTGATGTGGA	TCCTTCCATTCCATCTCCTG
B^0AT1 (*Slc6a19*)	5'-CATGATCCCATTCCTCATCC-3'	5'AGTACAGGCCCACCATGAAG-3'
SNAT3 (*Slc38a3*)	5'-CTGCTGAGGCCTTCTGTACC-3'	5'-GCAATGGACAGGTTGGAGAT-3'
LAT2 (*Slc7a8*)	5'-GGAGAGTGGAGGTGCCATTA-3'	5'-TGGTTCCCTGGAGAATGAAG-3'
PEPCK (*Pck1*)	5'-AGCCTTTGGTCAACAACTGG-3'	5'-TGCCTTCGGGGTTAGTTATG-3'
PDG (*Gls2*)	5'-GACCCTCACTACCTGC-3'	5'-GTCCCTGCGTAGGATG-3'
GDH (*Gdh*)	5'-GTGGCATGGTCCTCAA-3'	5'-CGCCCCATAGTGCTAC-3'
Genotyping: Targeted DNA		
Endogenous *Kcnj15*	5'-TTGCTGCCACCTTTGTGATGACCTG-3'[a]	5'-GGAAGATAGCATGGGGACACTCCTC-3'[b]
Inserted *LacZ-Neo*	5'-GGGTGGGATTAGATAAATGCCTGCTCT-3'[c]	5'-GGAAGATAGCATGGGGACACTCCTC-3'[b]

Table S3. Primers used for RT-qPCR on whole kidneys and nephron segments extracts and for mice genotyping. Primers used for genotyping were as per Deltagen's instructions. [a] and [b] : codons 70-78 and 137-144 of the endogenous *Kcnj15* mouse gene, respectively. [c] is complementary of the 3' sequence of the inserted Neomycin-resistance (*LacZ-Neo*) gene.

Supplementary methods.

Generation of *Kcnj15*$^{-/-}$ mice. SPF breeding nucleus B6;129P2-Kcnf15^{tm1Dgen}/H strain heterozygous mice of mixed 129P2/OlaHsd and C57BL/6J background (Deltagen, San Mateo, CA, USA) were obtained from the MRC Harwell, Mary Lyon Centre (Oxford, GB). Nucleus mice contained a mutant allele generated by the intragenic deletion of 136 bases (267-402) in exon 4 of the *mus musculus Kcnj15* DNA sequence, encoding a 46 amino-acids region ranging from the end of the first membrane-spanning hydrophobic domain (M1) to the pore-forming (H5) domain of the predicted Kir4.2 protein,[S1] and by the insertion of a promotorless *LacZ* reporter gene and a neomycin-resistant gene cassette (*LacZ-Neo*) flanked by 4.5 Kb (5′) and 2.5 Kb (3′) *Kcnj15* genomic DNA fragments homology arms (Figure S7A and S7B). The breeding of nucleus *Kcnj15*$^{+/-}$ mice with C57Bl/6 mice (Charles River Laboratories, Saint-Germain-sur-l'Arbresle, France) and the backcrossing of their heterozygous offspring onto a pure C57BL/6 background was then done to produce N5 generation of mice.

The intercrossing of *Kcnj15*$^{+/-}$ mice resulted in offspring of usual litter sizes with sex-ratios of *Kcnj15*$^{+/+}$, *Kcnj15*$^{+/-}$ and *Kcnj15*$^{-/-}$ mice at age of weaning close to 1:1 (160 males and 149 females) (Figure S7C). Genotype distribution roughly followed an expected mendelian inheritance pattern with ~30 % *Kcnj15*$^{+/+}$, ~44 % *Kcnj15*$^{+/-}$ and ~26 % *Kcnj15*$^{-/-}$ mice. Of the male offspring, ~28 % were homozygous, ~44 % heterozygous and ~28 % *Kcnj15*$^{+/+}$ mice, and female offspring distribution was ~23 % homozygous, ~44 % heterozygous and ~32 % *Kcnj15*$^{+/+}$ mice.

Mice genotype was established by multiplex PCR on ethanol-purified genomic DNA from tail biopsies according to Deltagen's instructions. PCR parameters were 94 °C for 3 min, 35 cycles at 94 °C for 10 sec, 60 °C for 30 sec, 72 °C for 1.5 min, and 72 °C for 7 min and the primers (Eurogentec, Angers, France) used are listed in Table S3. PCR products were separated on a 1.4 % agarose gel along a Invitrogen™ 100bp DNA ladder (ThermoFisher Scientific, Villebon sur Yvette, France) and visualized using ethidium bromide. Endogenous *Kcnj15* and targeted alleles were identified by amplification of 224-bp and 430-bp fragments, respectively.

Urine and blood analyses. 24-hour urine samples were collected under water-saturated mineral oil for urine NH_4^+ concentration and titratable acidity determination by a DL55 titrator and a ST20 sample changer (Mettler Toledo, Viroflay, France) and for HCO_3^- content measurement by a ABL 720 analyzer (Radiometer, Neuilly-Plaisance, France). Venous blood

from the retro-orbital plexus of conscious mice was analyzed by a blood gas epoc® Reader and Host analyzer (Alere S.A.S., Jouy en Josas, France) for determinations of pH, gas contents and haematocrit, and of Na^+, HCO_3^-, Cl^-, ionized Ca^{2+}, and glucose concentrations. At the end of the experimental period, mice were sacrificed by terminal bleeding after the peritoneal injection of ketamine and xylazine (0.12 and 0.006 mg/g body weight, respectively) and blood samples were collected on heparin for measurements of plasma creatinine by a Konelab 20I analyzer (ThermoFisher Scientific) and of K^+ concentration by a Sherwood 420 flame photometer (Servilab, Le Mans, France). Urinary Na^+ and K^+ contents were measured by flame photometry and urinary aldosterone by a ELISA Kit (Uscn Life Science Inc., Wuhan, China). Glomerular filtration rates were estimated using measured urine and plasma creatinine contents and urine volumes.

Real-time PCR on whole kidneys. Whole kidney mRNAs were extracted using the TRI Reagent® (ThermoFisher Scientific), treated with the RNAse Free DNAse Set and purified using the RNeasy Mini Kit (Qiagen, Courtaboeuf, France). 1 µg of purified mRNA was reverse-transcribed using the first strand cDNA synthesis kit for RT-PCR (Roche Diagnostics, Meylan, France). Real-time PCR was then performed with a LIGHTCYCLER® 480 using LC 480 SYBR Green 1 Master kit (Roche Diagnostics) in a 10 µl reaction volume, by 45 cycles of 20 seconds temperatures steps at 95 °C, 60 °C, and 72 °C, using the primers listed in Table S3.

Immunohistochemistry on kidney slices. Kidneys of anesthetized mice were fixed by transcardial perfusion with 4 % paraformaldehyde-containing PBS, harvested, washed in ice cold PBS and snap-frozen into liquid-nitrogen-cold isopentane. At the time of the experiment, 7 µm-thick sagittal sections were cut with a CM3050S cryostat (Leica Biosystems, Nanterre, France), blocked with 10 % normal goat serum, then exposed overnight at 4 °C to the APC-058 rabbit anti-Kir4.2 (1:500 dilution) primary antibody (Alomone Labs, Jerusalem, Israel) whose immunogen sequence targets the intracellular C-terminal region of the protein (hence outside the deleted part in *Kcnj15*$^{-/-}$ mice). After three washings with PBS, sections were exposed for 2 hours at room temperature to the A31572 donkey anti rabbit AlexaFluor® 555 (ThermoFisher Scientific, Villebon sur Yvette, France; 1:1000 dilution), DAPI (1 µg/ml) and Acti-Stain® 488 Fluorescent Phalloidin (Cytoskeleton, Denver, CO, USA; 1:250 dilution) secondary antibody then washed before mounting in Dako Glycergel mounting medium (Agilent Technologies, Les Ulis, France).

Protein extraction. For western blot experiments, mouse kidneys snap-frozen into liquid-nitrogen were mechanically homogenized and incubated in a ice-cold lysis buffer containing in mM 150 NaCl, 50 Tris, 1 EDTA supplemented with respectively 0.1 % SDS and 1 % Triton-X100 or 0.2 % SDS and 1 % NP-40. For co-immunoprecipitation experiments, protein extraction was performed on freshly retrieved kidneys using lysis buffer supplemented with 0.02 % sodium azide and 0.5 % sodium-deoxycholate.[S2] All lysis buffers were enriched with 1X cOmplete™ EDTA Free Protease Inhibitor Cocktail (Roche Diagnostics). After a centrifugation at 5,000 g for 10 minutes, protein content of supernatants was measured using the Pierce™ BCA Protein Assay Kit (ThermoFischer Scientific).

Western blotting. 60 µg proteins were denaturated in a 2X Laemmli buffer containing 2.5 % β-mercapto-ethanol, 5 % SDS and 13.6 % sucrose. All but Kir4.2 proteins were incubated in this medium for 10 minutes at 95 °C. Kir4.2 proteins were subjected to a mild three-steps procedure (15 min at 50 °C, 30 min at 25 °C and 15 min at 50 °C), as used for SDS-resistant GIRK4 channel,[S3] and shown to increase mobility and migration of the Kir4.2 protein into the polyacrylamide gel.[S4] Proteins were then separated on 0.5 % SDS, 10% polyacrylamide gels, transfered onto nitrocellulose membranes, blocked using a TBS buffer supplemented with 5 % non-fat milk proteins and 0.2 % NP-40, then exposed to primary antibody, washed and finally exposed to the following HRP-conjugated secondary antibody: 170-6515 goat anti-rabbit (Biorad, Marnes-la-Coquette, France; 1:2500 dilution, except 1:10000 dilution for NHE3 detection), sc-2020 donkey anti-goat (1:5000 dilution) and sc-2005 goat anti-mouse (1:10000 dilution) (Santa Cruz Biotechnologies, CliniSciences, Nanterre, France).

The primary antibodies used were: APC-058 rabbit anti-Kir4.2, SPC-400D rabbit anti-NHE3 (StressMark Biosciences, Victoria, Canada; 1:2000 dilution), ab187511 rabbit anti-NBCe1 (Abcam, Paris, France; 1:2500 dilution), APC-037 rabbit anti-TASK2 (Alomone Labs, 1:1000 dilution), sc-33445 goat anti-SNAT3 (Santa Cruz Biotechnology, Santa Cruz, CA, USA, 1:1000 dilution), Cayman Chemical 10004943 rabbit anti-PEPCK (Bertin Bioreagent, Montigny le Bretonneux, France, 1:5000 dilution) and A2228 mouse anti-β-Actin (Sigma Aldrich Chemie; 1:20000 dilution). The rabbit anti-PDG (1:5000 dilution) was kindly provided by Pr Javier Marquez (University of Malaga, Spain)

Membrane potential measurement. Tubules were isolated from kidneys after a collagenase treatment as previously described,[S5] then transferred into a chamber placed on the

stage of an inverted microscope. The bath solution contained (mM) 130 NaCl, 5 KCl, 2 NaH_2PO_4, 10 Na-acetate, 2 L-Alanine, 1 $CaCl_2$, 1 $MgCl_2$, 10 HEPES, 10 glucose and was adjusted to pH 7.4 with tris(hydroxymethyl)aminoethane. Patch pipettes were pulled from thin-walled borosilicate glass capillaries (Phymep, Paris, France), heat polished and backfilled with the bath solution. Immersing the pipette tip into the bath yield a resistance of ~ 5 MΩ and any residual liquid junction potential or headstage offset current was carefully cancelled. After the establishment of a stable tight seal on the basolateral membrane, the voltage signal measured by a RK400 patch clamp amplifier (Bio-Logic Science Instruments, Seyssinet-Pariset, France) set in the zero current-clamp (I0) mode was filtered at 50 Hz by a NPI Electronic LPBF-48DG low-pass 8-pole Bessel filter (Tamm, Germany) and digitized at a 100 Hz sampling rate by an Axon Instruments/Molecular Devices Digidata 1440A A/D converter and P-clamp software (Dipsi Industrie, Châtillon, France). All experiments were performed at room temperature (20-25°C).

Intracellular pH measurements. Dye-loaded tubules were excited alternatively at 440 and 500 nm (BW 20 nm) every 2 seconds with an OptoLED light source (Cairn Research, Faversham, GB) and an iXon EMCCD camera (Andor Technology, Belfast, GB) collected the light emitted at 530 nm. Fluorescence images were acquired at a 14 bit-depth and stored for further analysis. The mean background-substracted gray levels at each excitation wavelength were measured with the Andor IQ software, ratioed and converted into pH units using a 4-point calibration by the high $[K^+]$-nigericin procedure performed at the end of each measurement.

Proximal tubules were superfused with either a Na^+-containing solution (119 mM NaCl, 23 mM $NaHCO_3$, 2 mM K_2HPO_4, 1.5 mM $CaCl_2$, 1.2 mM $MgSO_4$, 5 mM L-Alanine, 5.5 mM D-glucose and 10 mM HEPES) or a nominally Na^+-free solution in which NMDG-Cl and NMDG-HCO_3 were substituted for NaCl and $NaHCO_3$, respectively. The tubular lumen was perfused with the Na^+-free solution all throughout the measurements to minimize the contribution of the apical Na^+/H^+ exchanger to the intracellular pH responses. All solutions were continuously gassed with 95% O2/5% CO_2 (pH ~7.40) and kept at 37°C.

S1. Pearson WL, Dourado M, Schreiber M *et al.* Expression of a functional Kir4 family inward rectifier K+ channel from a gene cloned from mouse liver. *J. Physiol.* 1999; **514 (Pt 3)**: 639–653.
S2. Tanemoto M, Kittaka N, Inanobe A *et al.* In vivo formation of a proton-sensitive K+ channel by heteromeric subunit assembly of Kir5.1 with Kir4.1. *J. Physiol.* 2000; **525 Pt 3**: 587–592.

S3. Corey S, Clapham DE. Identification of native atrial G-protein-regulated inwardly rectifying K+ (GIRK4) channel homomultimers. *J. Biol. Chem.* 1998; **273**: 27499–27504.
S4. Hill CE, Briggs MM, Liu J *et al.* Cloning, expression, and localization of a rat hepatocyte inwardly rectifying potassium channel. *Am. J. Physiol. Gastrointest. Liver Physiol.* 2002; **282**: G233-240.
S5. Paulais M, Lachheb S, Teulon J. A Na+- and Cl- -activated K+ channel in the thick ascending limb of mouse kidney. *J. Gen. Physiol.* 2006; **127**: 205–215.

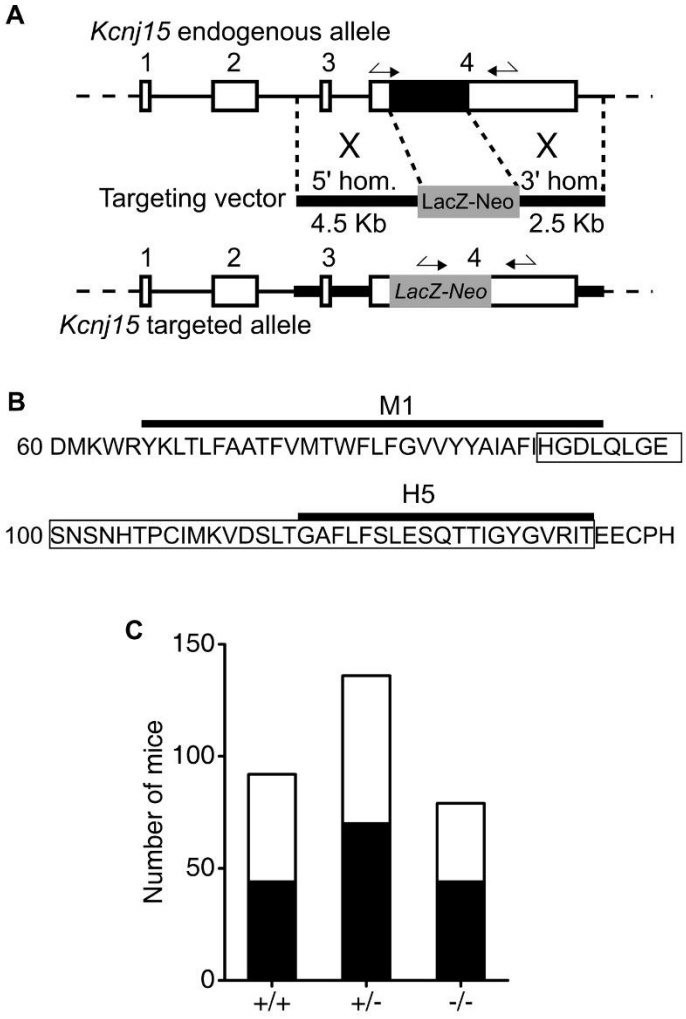

Figure S7. *Kcnj15* deletion. (**A**) *Kcnj15* endogenous allele, targeting vector, and targeted alleles. The 136 bases deleted region in exon 4 of the endogenous allele is shown as a black box. Numbers indicate *Kcnj15* exons (open boxes). The thick lines represent fragments used for constructing the *LacZ-Neo* targeting vector 4.5 Kb (5′) and 2.5 Kb (3′) homology arms. Arrows indicate the PCR primers used for the genotyping shown in (C). (**B**) The corresponding deleted deduced amino-acids sequence of Kir4.2 protein (hollow box) covers a region from the end of the proposed first membrane-spanning hydrophobic segment (M1) to the pore-forming region domain (H5). (**C**) $Kcnj15^{+/+}$, $Kcnj15^{+/-}$ and $Kcnj15^{-/-}$ offspring genotypes from heterozygous mating roughly followed mendelian distribution and, for each genotype, male (black bars) to female (open bars) ratios approached 1:1.